Received: 28 December 2020 | Revised: 23 February 2021 | Accepted: 26 February 2021

DOI: 10.1002/ardp.202000491

FULL PAPER

ARCH PHARM DPhG
Archiv der Pharmazie

Design, synthesis, docking, ADMET profile, and anticancer evaluations of novel thiazolidine-2,4-dione derivatives as VEGFR-2 inhibitors

Khaled El-Adl[1,2] | Helmy Sakr[1] | Sanadelaslam S. A. El-Hddad[1] | Abdel-Ghany A. El-Helby[1] | Mohamed Nasser[1] | Hamada S. Abulkhair[3,4]

[1]Pharmaceutical Medicinal Chemistry and Drug Design Department, Faculty of Pharmacy (Boys), Al-Azhar University, Nasr City, Cairo, Egypt

[2]Pharmaceutical Chemistry Department, Faculty of Pharmacy, Heliopolis University for Sustainable Development, El-Salam City, Cairo, Egypt

[3]Pharmaceutical Organic Chemistry Department, Faculty of Pharmacy (Boys), Al-Azhar University, Nasr City, Cairo, Egypt

[4]Pharmaceutical Chemistry Department, Faculty of Pharmacy, Horus University, New Damietta, Egypt

Correspondence

Khaled El-Adl, Pharmaceutical Medicinal Chemistry and Drug Design Department, Faculty of Pharmacy (Boys), Al-Azhar University, Nasr City 11884, Cairo, Egypt.
Email: eladlkhaled74@yahoo.com and eladlkhaled74@azhar.edu.eg or khaled.eladl@hu.edu.eg

Abstract

The anticancer activity of novel thiazolidine-2,4-diones was evaluated against HepG2, HCT-116, and MCF-7 cells. Among the tested cancer cell lines, HCT-116 was the most sensitive one to the cytotoxic effect of the new derivatives. In particular, compounds **18**, **11**, and **10** were found to be the most potent derivatives among all the tested compounds against the HepG2, HCT-116, and MCF-7 cancer cell lines, with IC_{50} values ranging from 38.76 to 53.99 μM. The most active antiproliferative derivatives (**7**–**14** and **15**–**19**) were subjected to further biological studies to evaluate their inhibitory potentials against VEGFR-2. The tested compounds displayed a good-to-medium inhibitory activity, with IC_{50} values ranging from 0.26 to 0.72 μM. Among them, compounds **18**, **11**, and **10** potently inhibited VEGFR-2 at IC_{50} values in the range of 0.26–0.29 μM, which are nearly three times that of the sorafenib IC_{50} value (0.10 μM). Although our derivatives showed lower activities than the reference drug, they could be useful as a template for future design, optimization, adaptation, and investigation to produce more potent and selective VEGFR-2 inhibitors with higher anticancer analogs. The ADMET profile showed that compounds **18**, **11**, and **10** do not violate any of Lipinski's rules and have a comparable intestinal absorptivity in humans. Also, the new derivatives could not inhibit cytochrome P3A4. Unlike sorafenib and doxorubicin, compounds **18**, **11**, and **10** are expected to have prolonged dosing intervals. Moreover, compounds **10** and **18** displayed a wide therapeutic index and higher selectivity against cancer cells as compared with their cytotoxicity against normal cells.

KEYWORDS

anticancer agents, HCT-116, HepG2, MCF-7, molecular docking, thiazolidine-2,4-dione, VEGFR-2 inhibitors

1 | INTRODUCTION

The molecular hybridization of the thiazolidine-2,4-diones (TZDs) scaffold with different bioactive moieties has recently been proposed to have a different mechanism of action with a broad spectrum of activities against numerous cancer cell lines. TZDs have exhibited an antitumor activity in a wide variety of experimental cancer models by affecting cell cycle, induction of cell differentiation, and apoptosis as well as by inhibiting tumor angiogenesis.[1] Angiogenesis, the process of formation of new blood vessels from the existing vasculature, is a fundamental event in tumor growth and metastasis.[2] Angiogenesis is one of the main molecular targets in recent developments in cancer therapies.[3] Newly generated blood vessels supply oxygen and essential nutrition, support tumor growth, and later aid in the initiation of metastasis, which contributes to more than 90% of deaths in various cancers.[4] Vascular endothelial growth factor (VEGF) is one of the central regulators in angiogenesis.[5] VEGFR-2 is the major mediator of VEGF-induced pro-angiogenesis signaling.[6] The binding of VEGF to VEGFR2 leads to activation of tyrosine kinase, *trans*-autophosphorylation, and initiation of the extracellular signal-regulated kinase.[7,8] Blockade of angiogenesis is one of the most promising strategies to treat malignancies. Shah et al.[9] reported that TZD derivative ciglitazone (**I**) (Figure 1) significantly decreased the VEGF production in human granulosa cells in an in vitro model. Extensive studies were reported on the synthesis of several 5-benzylidenethiazolidine-2,4-dione derivatives as potent anticancer agents[10–13] and potent VEGFR-2 inhibitors, for example, compound **II**.[9] Numerous reports on VEGFR-2 inhibitors, including the commercialized sunitinib (**III**) (Figure 1), have been published.[14,15] Sorafenib (Nexavar)® (**IV**) (Figure 1) is also a potent VEGFR-2 inhibitor and has been approved as an antiangiogenic drug.[16,17]

VEGFR-2 was reported to be markedly overexpressed in HCC (HepG2) cells.[18,19] Blockade of VEGFR-2 signaling revealed a noticeable inhibition of both the growth and metastasis of hepatocellular carcinoma (HCC).[19,20] Also, VEGFR-2 regulates endothelial differentiation and is essential to cell survival of both the human colorectal carcinoma (HCT-116)[21,22] and breast cancer cells (Michigan Cancer Foundation-7 [MCF-7]).[23,24] VEGFR-2 inhibitors were reported to impair the in vitro endothelial differentiation and to promote angiogenesis, suggesting a VEGFR-2-mediated mechanism of antiproliferative activity in human colorectal carcinoma.[21] The overexpression of VEGFR-2 receptors in breast cancer has been verified as a sponsor in the resistance of such cancer against the chemotherapeutic effect of tamoxifen.[23]

A study of the structure–activity relationships (SAR) and common pharmacophoric features shared by sorafenib and various VEGFR-2 inhibitors revealed that most VEGFR-2 inhibitors shared four main

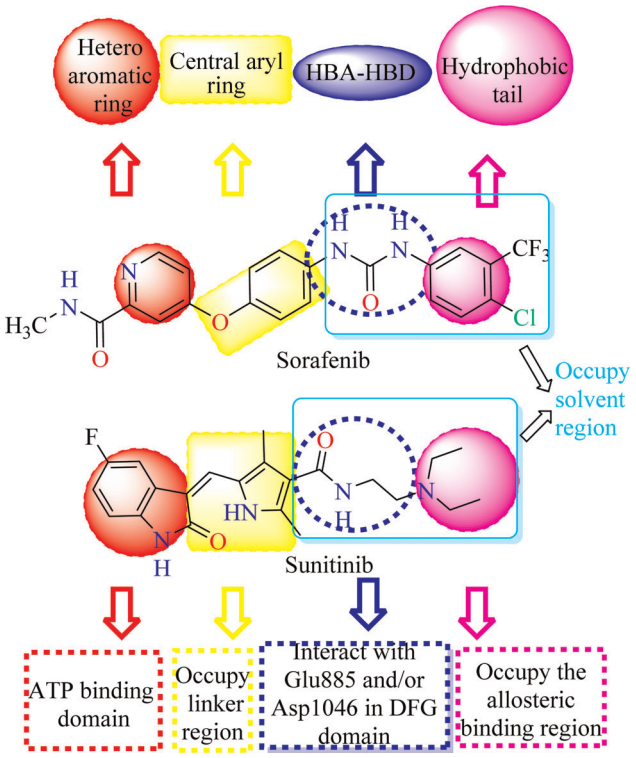

FIGURE 2 The basic structural requirements for sorafenib and sunitinib as reported VEGFR-2 inhibitors. ATP, adenosine triphosphate; HBA, hydrogen-bond acceptor; HBD, hydrogen-bond donor; VEGFR, vascular endothelial growth factor

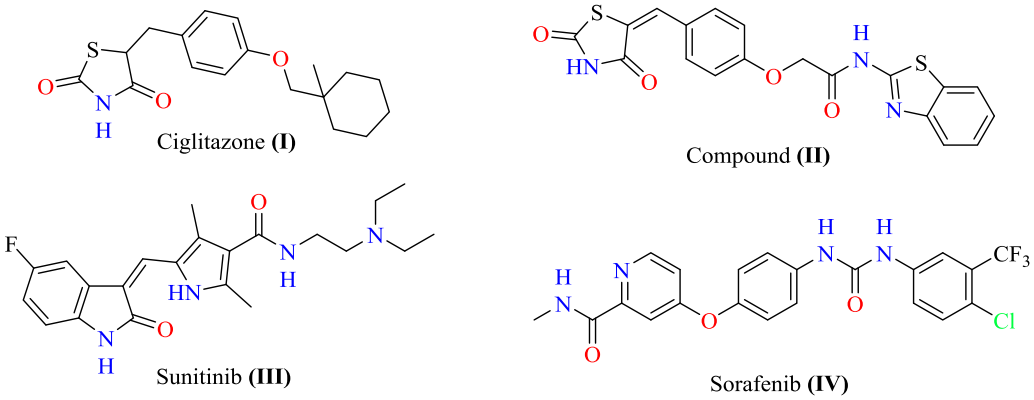

FIGURE 1 Reported vascular endothelial growth factor-2 inhibitors

features, as shown in Figure 2.[25,26] The first feature is the flat heteroaromatic ring system that contains at least one N-atom as the core structure of most inhibitors, which occupied the catalytic adenosine triphosphate (ATP)-binding domain. The second feature is a hydrophobic spacer (central aryl ring), occupying the linker region between the ATP-binding domain and the DFG domain of the enzyme.[27] The third one is a linker containing a functional group acting as a pharmacophore (e.g., amino or urea) that possesses both H-bond acceptor (HBA) and donor (HBD) to bind with two crucial residues (Glu885 and/or Asp1046) in the DFG (Asp–Phe–Gly) motif, an essential tripeptide sequence in the active kinase domain. The NH motifs of the urea or amide moiety usually form one hydrogen bond with Glu885, whereas the C═O motif forms another hydrogen bond with Asp1046. Finally, the fourth feature, the terminal hydrophobic moiety of the inhibitors occupies the newly created allosteric hydrophobic pocket. Thus, hydrophobic interactions are usually attained in this allosteric binding region.[28] The [4-chloro-3-(trifluoromethyl)phenyl]urea and *N*-[2-(diethylamino)ethyl]carboxamide tails of sorafenib and sunitinib, respectively, were located at the solvent region of the VEGFR-2 receptor. Furthermore, analysis of the X-ray structure of various inhibitors bound to VEGFR-2 confirmed the sufficient space available for various substituents around the terminal heteroaromatic ring.[29,30]

Depending on ligand-based drug design, especially a molecular hybridization approach that involves the coupling of two or more groups with relevant biological properties,[31–33] molecular hybridization of 5-[(4-chloro/2,4-dichloro)benzylidene]thiazolidine-2,4-diones and other effective antitumor moieties was carried out in an attempt to obtain new molecules with potent antitumor activity.

In view of the abovementioned findings and based on our continuous efforts to develop new anticancer agents,[70,34–39] especially VEGFR-2 inhibitors,[12,13,40–44] the goal of our work was to synthesize new agents with the same essential pharmacophoric features of the reported and clinically used VEGFR-2 inhibitors (e.g., sorafenib). The main core of our molecular design rationale comprised bioisosteric modification strategies of VEGFR-2 inhibitors at four different positions (Figure 3).

Our target compounds were designed to have different spacers and linkers while retaining the main pharmacophoric features of sorafenib, hoping to obtain more potent VEGFR-2 inhibitors. First, a bioisosteric approach was adopted in the target 4-chloro and/or 2,4-dichlorobenzylidenes to replace the hydrophobic group-substituted phenyl tail of the reported ligand sorafenib. The second strategy is to use TZD to replace the central aryl ring of the lead structure, aiming to increase the VEGFR-2 binding affinity. The third strategy is using

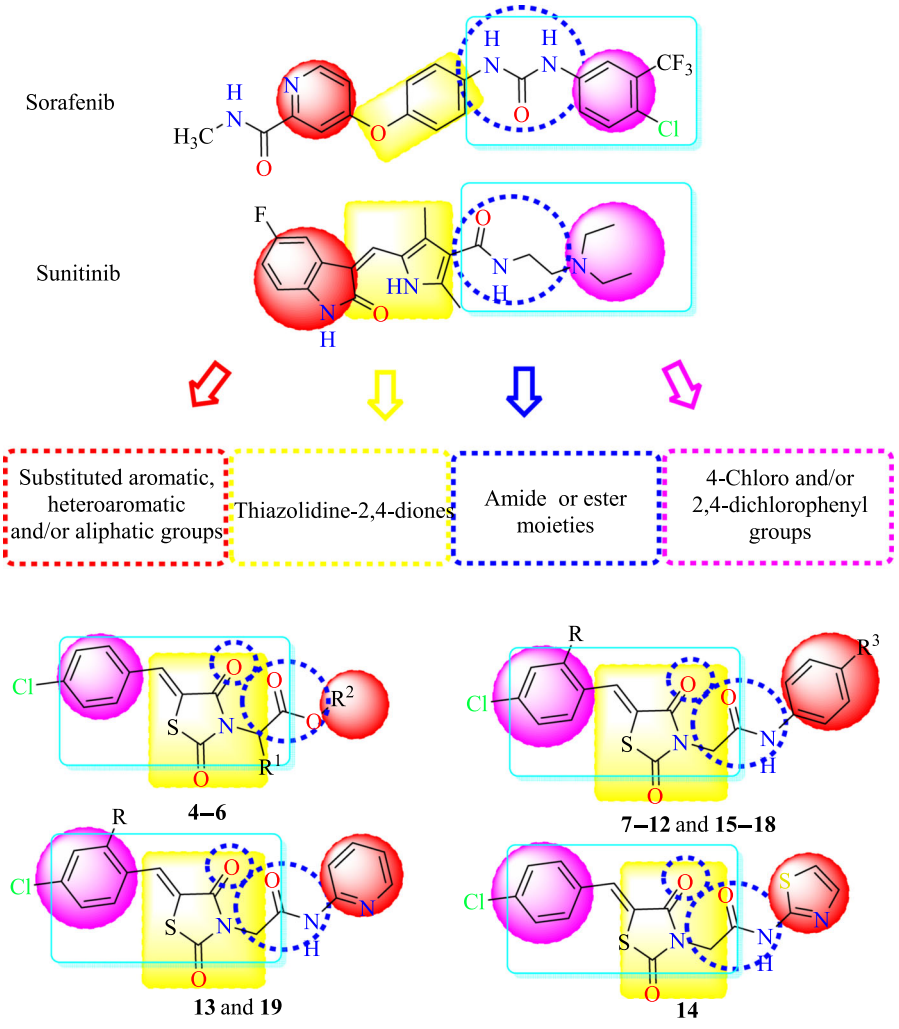

FIGURE 3 Structural similarities and pharmacophoric features of VEGFR-2 inhibitors and designed compounds. VEGFR, vascular endothelial growth factor-2

ester and/or acetamide linkers that contain HBA–HBD functional groups. In addition, the pyridine ring and indolin-2-one of sorafenib and sunitinib, respectively, were replaced by their bioisosteres, heteroaromatic, and/or substituted aromatic moieties. Lastly, the substitution pattern was selected to ensure different electronic and lipophilic environments that could influence the activity of the target compounds. These modifications were performed to carry out further elaboration of the TZD scaffolds and to explore a valuable SAR. The designed target derivatives were synthesized and evaluated as potential VEGFR-2 inhibitors and antitumor agents against three human tumor cell lines, namely HCC type (HepG2), breast cancer (MCF-7), and human colorectal carcinoma-116 (HCT-116).

2 | RESULTS AND DISCUSSION

2.1 | Rationale and structure-based design

5-[(4-Chloro/2,4-dichloro)benzylidene]thiazolidine-2,4-dione derivatives have the essential pharmacophoric features of VEGFR-2 inhibitors[15,44–48] (Figure 3), which include the following: the presence of five-membered heterocyclic rings, TZD, substituted with 4-chlorobenzylidene and/or 2,4-dichlorobenzylidene moieties, as hydrophobic portions, forming 5-(4-chlorobenzylidene)thiazolidine-2,4-dione and 5-(2,4-dichlorobenzylidene)-thiazolidine-2,4-dione scaffolds. These scaffolds are linked to (un)substituted hydrophobic moieties through ester and/or acetamide linkers containing HBA–HBD, which interact as an HBA through their C═O and as HBD through their NH atom with the essential amino acid residues Asp1046 and/or Glu885. Also, the heteroaromatic pyridine or thiazole and substituted phenyl rings with hydrophilic carboxylic and/or carboxamide groups were designed to replace the pyridine and 5-fluoro-2-oxoindolin-3-ylidene moieties of the reference ligands sorafenib and sunitinib, respectively. In addition, 4-chlorobenzylidene and 2,4-dichlorobenzylidine moieties were designed to replace the hydrophobic tails of the reference ligands sorafenib and sunitinib. Moreover, TZD was designed to replace the central aryl and pyrrole ring of the reference ligands. Furthermore, the hydrophobic 4-chlorobenzylidene and/or 2,4-dichlorobenzylidene moieties occupied the hydrophobic groove formed by Asp1046, Cys1045, Hie1026, Ile892, Ile888, and Glu885 (Figures 4 and 5).

2.2 | Chemistry

The adopted synthetic strategy for the preparation of the target compounds (**4**–**19**) is depicted in Scheme 1. The synthesis was initiated by cyclocondensation of thiourea with chloroacetic acid to afford TZD (**1**),[12,13] which underwent further condensation reaction with 4-chlorobenzaldehyde and/or 2,4-dichlorobenzaldehyde to afford 5-(4-chlorobenzylidene)thiazolidine-2,4-dione and/or 5-(2,4-dichlorobenzylidene)thiazolidine-2,4-dione (**$2_{a,b}$**), respectively. Heating the latter benzylidines with an alcoholic solution of potassium hydroxide afforded the corresponding potassium salts (**$3_{a,b}$**). The ester derivatives (**4**–**6**) were readily obtained by reacting the potassium salt **3_a** under reflux with the appropriate α-chloroester derivative.[49–54] However, α-chloroacetyl chloride was allowed to react with a variety of aromatic amines to obtain the corresponding α-chloro-*N*-arylamides.[35,55] Treating the potassium salt of **3_a** with the freshly prepared α-chloro-*N*-arylamides furnished the corresponding amide derivatives **7**–**14**.[44,56–58] Alternatively, the potassium salt **3_b** was refluxed with the same set of α-chloro-*N*-arylamides derivatives to afford our target amide derivatives **15**–**19**.

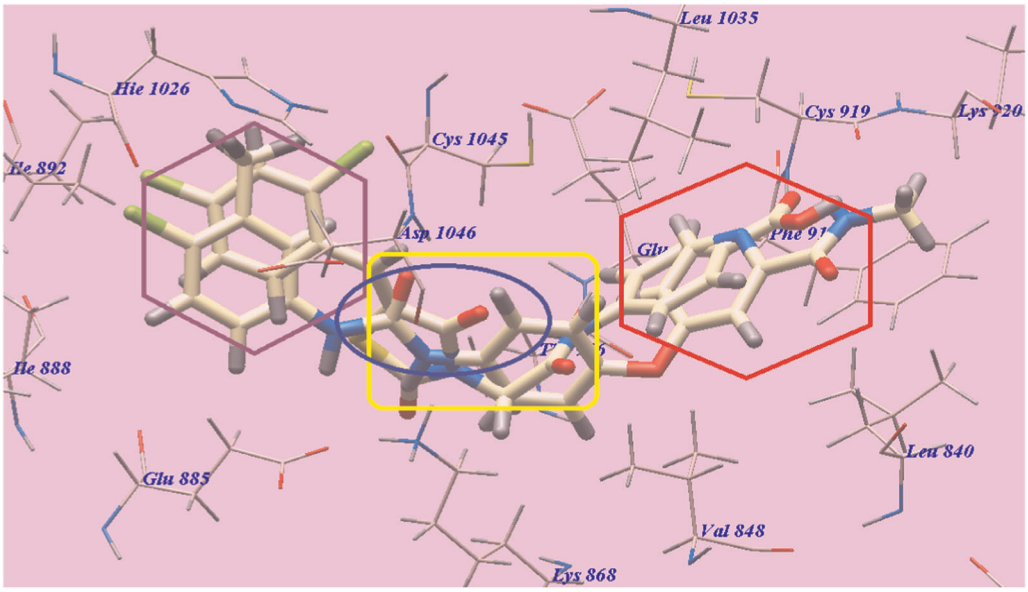

FIGURE 4 Superimposition of compound **18** and sorafenib inside the binding pocket of 3B8Q

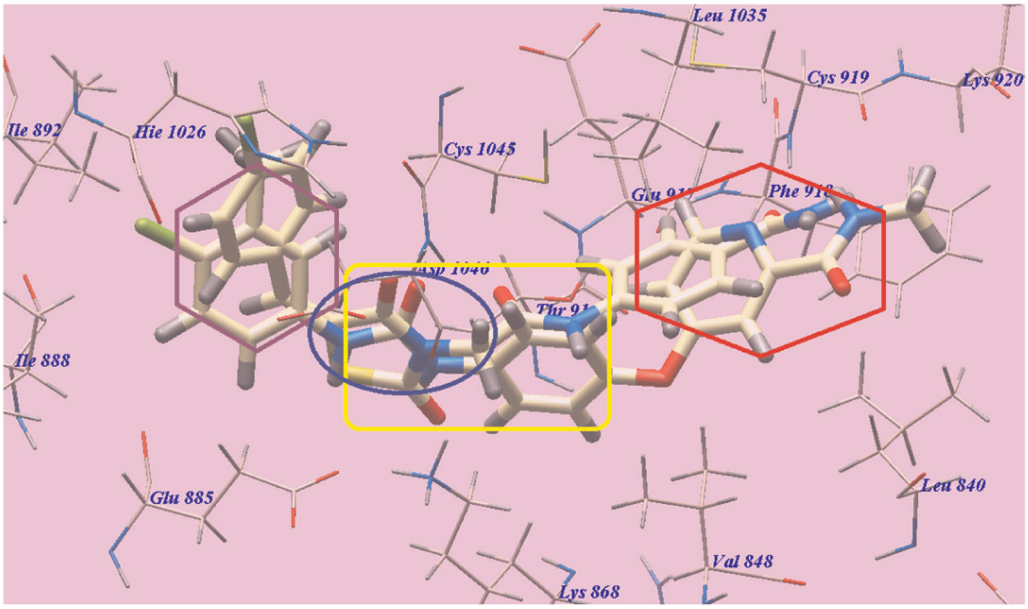

FIGURE 5 Superimposition of compound **11** and sorafenib inside the binding pocket of 3B8Q

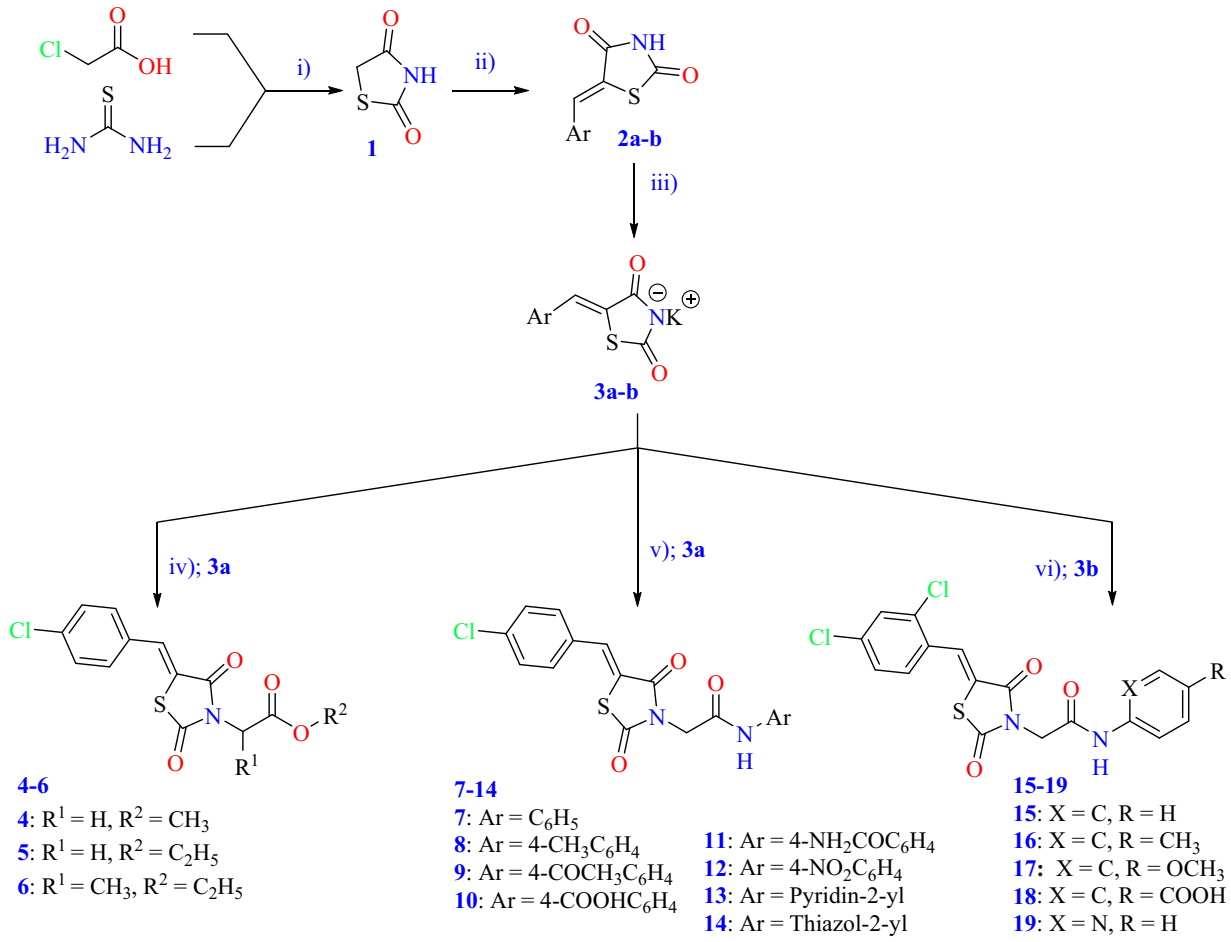

SCHEME 1 Synthetic route for the preparation of the target compounds **4–19**. Reagents and conditions: (i) HCl, 90°C, 3 h, 90%; (ii) ArCHO/AcOH/AcONa, 90°C, 3 h, 74–80%; (iii) KOH/C_2H_5OH, 90°C, 1h, 95%; (iv) $ClCH(R^1)COOR^2$/DMF/K_2CO_3, water bath, 5 h, 81–90%; (v) ClH_2CONH–Ar/DMF/K_2CO_3, water bath, 4 h, 55–92%; (vi) $ClCH_2CONH$–Ar/DMF/K_2CO_3, water bath, 4 h, 60–70%. DMF, dimethylformamide

The process of chemical reactions was monitored by the thin-layer chromatography (TLC) approach. The structure and purity of each new derivative were confirmed on the basis of spectral data and elemental analysis. In all cases, a new typical ester and amide carbonyl stretching bands between 1681 and 1693 cm^{-1} were observed in the infrared (IR) spectra. These findings confirm the tethering of the ester and acetanilide fragments with the TZD nucleus. The amidic NH group revealed a D_2O-exchangeable signal at the range of 10.32–11.05 ppm in ^1H nuclear magnetic resonance (NMR) spectra of compounds **7**–**14** and **15**–**19**. Also, IR spectra of these amides showed stretching bands in the range of 3232 and 3282 cm^{-1}, signifying the secondary amide NH functionality. The most principal feature in the IR and ^1H NMR spectra of the ester derivatives **4**–**6** was the appearance of a distinctive carbonyl ester stretching band around 1790 cm^{-1} and the protons of added alkyl ester moieties with their relevant signals between 1.22 and 4.53 ppm.

2.3 | In vitro cytotoxic activity

The antiproliferative activity of the newly synthesized TZD derivatives **4**–**19** was examined against three human tumor cell lines, namely HCC (HepG2), colorectal carcinoma (HCT-116), and breast cancer (MCF-7), using 3-[4,5-dimethylthiazol-2-yl]-2,5-diphenyltetrazolium bromide (MTT) colorimetric assay, as described by Mosmann.[59] Sorafenib and doxorubicin were included in the experiments as reference cytotoxic drugs. The results were expressed as growth inhibitory concentration (IC_{50}) values, which represent the compound concentrations required to produce a 50% inhibition of cell growth after 72 h of incubation, calculated from the concentration–inhibition response curve and summarized in Table 1. From the obtained results, it was explicated that most of the prepared compounds displayed a good-to-low growth inhibitory activity against the tested cancer cell lines. Investigations of the cytotoxic activity indicated that HCT-116 was the cell line most sensitive to the influence of the new derivatives. In particular, compounds **18**, **11**, and **10** were found to be the most potent derivatives among all the tested compounds against HepG2, HCT-116, and MCF-7 cancer cell lines, with IC_{50} = 38.76 ± 2.9, 43.54 ± 4.4, 50.13 ± 3.5 μM; 40.26 ± 3.3, 48.34 ± 4.5, 52.34 ± 3.7 μM; and 42.34 ± 3.2, 46.26 ± 4.7, 53.99 ± 3.7 μM, respectively.

With respect to the HepG2 HCC cell line, compounds **17**, **9**, **13**, **16**, **19**, **15**, and **12** displayed modest anticancer activities, with IC_{50} = 52.86 ± 3.7, 53.75 ± 3.9, 64.19 ± 4.2, 65.98 ± 4.8, 70.11 ± 6.1, 71.02 ± 3.8, and 72.72 ± 4.6 μM, respectively. Compounds **7**, **8**, and **14** with IC_{50} values ranging from 82.69 ± 4.8 to 94.35 ± 5.2 μM exhibited the lowest cytotoxicity. However, compounds **4**, **5**, and **6** with IC_{50} >100 showed no cytotoxic activity.

Cytotoxicity evaluation against colorectal carcinoma (HCT-116) cell line revealed that compounds **17**, **9**, and **7** displayed good anticancer activities with IC_{50} = 43.66 ± 4.5, 44.34 ± 3.3, and 50.42 ± 3.5 μM, respectively. Compounds **8**, **12**, **13**, **14**, **15**, **16**, and **19** displayed modest anticancer activities with IC_{50} values ranging from 54.50 ± 2.8 to 74.79 ± 4.3 μM. Compounds **6** and **5** with IC_{50} = 83.91 ± 4.9 and 91.67 ± 5.3 μM, respectively, exhibited the lowest cytotoxicity. However, compound **4** with IC_{50} >100 showed no cytotoxic activity.

Cytotoxicity evaluation against MCF-7 cell line revealed that compounds **17** and **16** displayed good anticancer activities with IC_{50} = 43.20 ± 4.5 and 49.87 ± 4.6 μM, respectively. Compounds **19**, **9**, **15**, **12**, and **13** with IC_{50} = 55.38 ± 4.1, 58.65 ± 3.8, 59.34 ± 3.9, 71.28 ± 4.5, and 75.85 ± 4.9 μM, respectively, displayed modest cytotoxicity. Compounds **8**, **14**, and **7** with IC_{50} = 77.36 ± 4.9, 89.06 ± 3.8, and 90.27 ± 5.2 μM, respectively, exhibited the lowest cytotoxicity. However, compounds **4**, **5**, and **6** with IC_{50} >100 showed no cytotoxic activity.

TABLE 1 In vitro cytotoxic activities of the newly synthesized compounds against HepG2, HCT-116, and MCF-7 cell lines and VEGFR-2 kinase assay

Compound	IC_{50} (μM)[a]			
	HepG2	HCT-116	MCF-7	VEGFR-2
4	>100	>100	>100	NT[b]
5	>100	91.67 ± 5.3	>100	NT[b]
6	>100	83.91 ± 4.9	>100	NT[b]
7	94.35 ± 5.2	50.42 ± 3.5	90.27 ± 5.2	0.67 ± 0.03
8	82.69 ± 4.8	57.56 ± 3.0	77.36 ± 4.9	0.61 ± 0.03
9	53.75 ± 3.9	44.34 ± 3.3	58.65 ± 3.8	0.34 ± 0.06
10	42.34 ± 3.2	46.26 ± 4.7	53.99 ± 3.7	0.29 ± 0.03
11	40.26 ± 3.3	48.34 ± 4.5	52.34 ± 3.7	0.28 ± 0.03
12	72.72 ± 4.6	69.87 ± 4.1	71.28 ± 4.5	0.68 ± 0.03
13	64.19 ± 4.2	54.50 ± 2.8	75.85 ± 4.9	0.63 ± 0.05
14	92.35 ± 5.2	63.85 ± 2.5	89.06 ± 3.8	0.72 ± 0.03
15	71.02 ± 3.8	74.79 ± 4.3	59.34 ± 3.9	0.62 ± 0.02
16	65.98 ± 4.8	62.09 ± 4.8	49.87 ± 4.6	0.49 ± 0.04
17	52.86 ± 3.7	43.66 ± 4.5	43.20 ± 4.5	0.32 ± 0.02
18	38.76 ± 2.9	43.54 ± 4.4	50.13 ± 3.5	0.26 ± 0.03
19	70.11 ± 6.1	65.02 ± 4.2	55.38 ± 4.1	0.58 ± 0.05
Sorafenib	9.18 ± 0.6	5.47 ± 0.3	7.26 ± 0.3	0.10 ± 0.02
Doxorubicin	7.94 ± 0.6	8.07 ± 0.8	6.75 ± 0.4	NT[b]

[a]IC_{50} values are the mean ± *SD* of three separate experiments.
[b]NT: Compounds not tested for their VEGFR-2 inhibitory activity.

2.4 | In vitro VEGFR-2 kinase assay

The newly synthesized 5-(4-chlorobenzylidene)thiazolidine-2,4-dione derivatives **7**–**14** and 5-(2,4-dichlorobenzylidene)-thiazolidine-2,4-dione derivatives **15**–**19** were evaluated for their inhibitory activities against VEGFR-2 by using an anti-phosphotyrosine antibody with the AlphaScreen system (PerkinElmer). The results were reported as a 50% inhibition concentration value (IC_{50}), calculated from the concentration–inhibition response curve and summarized in Table 1.

Sorafenib was used as a positive control in this assay. The tested compounds displayed a good-to-medium inhibitory activity with IC_{50} values ranging from 0.26 ± 0.03 to 0.72 ± 0.03 μM. Among them, compounds **18**, **11**, and **10** potently inhibited VEGFR-2 at IC_{50} values of 0.26 ± 0.03, 0.28 ± 0.03, and 0.29 ± 0.03 μM, respectively, which are nearly more than one-third of that of sorafenib IC_{50} value (0.10 ± 0.02 μM). Also, compounds **17**, **9**, and **16** possessed good VEGFR-2 inhibition with IC_{50} values of 0.32 ± 0.02, 0.34 ± 0.06, and 0.49 ± 0.04 μM, respectively. However, compounds **7**, **8**, **12**, **13**, **14**, **15**, and **19** exhibited moderate VEGFR-2 inhibition with IC_{50} values ranging from 0.58 ± 0.05 to 0.72 ± 0.03 μM.

2.5 | SAR

The preliminary SAR study has focused on the effect of replacement of the urea and carboxamide linkers of sorafenib and sunitinib, respectively, with acetamide linkers of our compounds, which interact as HBAs through their carbonyl group and as HBD through their NH atom. These acetamide linkers interact with the side chain NH of the essential amino acid residue Asp1044 and carboxylate of the essential amino acid residue Glu883. Also, our derivatives formed hydrophobic interactions through the attached hydrophobic moieties. The effect of replacement of pyridine and 5-fluoro-2-oxoindolin-3-ylidene moieties of sorafenib and sunitinib, respectively, with the 4-chlorobenzylidene and/or 2,4-dichlorobenzylidene on the antitumor activities also was noticed. These 5-(4-chloro/2,4-dichloro)benzylidene moieties occupied the same hydrophobic pocket that was occupied by the pyridine moiety of the standard ligand. Moreover, the TZD was designed to replace the central aryl and pyrrole ring of the reference ligands sorafenib and sunitinib, respectively, and enable the target compounds to form new H-bonds through their 2-carbonyl groups with the essential amino acid residue Lys866. The data obtained revealed that the tested compounds displayed different levels of anticancer activity and possessed a distinctive pattern of selectivity against the HCT-116 cell lines. Generally, the spacers, linkers (HBA–HBD), lipophilicity, and electronic nature of substituents exhibited an important role in anticancer activity. The 2,4-dichlorobenzylidene moiety exhibited higher anticancer activities than the 4-chlorobenzylidene moiety, which may be attributed to the higher lipophilicity of two lipophilic chloro atoms.

From the structure of the synthesized derivatives and the data shown in Table 1, we can divide these tested compounds into three groups. The first group consists of compounds **4**–**6**, where ethyl propionate ester derivative **6** showed higher activities than the ethyl acetate **5** and the methyl one **4**. In the second group, **7**–**14**, the terminal phenyl tails were replaced by another heteroaromatic pyridine ring, as in compound **13**, and/or thiazole ring, as in compound **14**. In the other derivatives, terminal phenyl tails were replaced with an (un)substituted phenyl, as in compound **7**, or *para*-substituted with different hydrophobic, hydrophilic, electron-donating, and/or electron-withdrawing groups. Generally, compounds with more hydrophilic electron-withdrawing substituents, for example, **11**, **10**, and **9**, showed higher activities than that with the hydrophobic electron-donating one, **8**, and the unsubstituted one, **7**, against the cell lines HepG2, HCT-116, and MCF-7. Compound **11** with carboxamide substitution exhibited higher activities than **10** with carboxylic and **9** with acetyl substitution against both HepG2 and MCF-7 cell lines, respectively, but it displayed a lower activity against HCT-116 cell line. The electron-withdrawing nitro derivative **12** displayed higher activities than that with the electron-donating methyl one, **8**, and the unsubstituted one, **7**, against both HepG2 and MCF-7 cell lines, respectively, but it displayed a lower activity against HCT-116 cell line. Furthermore, the terminal pyridine tail, as in compound **13**, exhibited higher activities than thiazole, as in compound **14**, and the phenyl tail **7** against both HepG2 and MCF-7 cell lines, respectively, but it displayed a lower activity against HCT-116 cell line.

In the third group, **15**–**19**, the terminal phenyl tails were replaced by another heteroaromatic pyridine ring, as in compound **19**. In the other derivatives, they were unsubstituted, as in compound **15**, and 4-substituted with different hydrophobic, hydrophilic, electron-donating, and/or electron-withdrawing groups. Generally, compounds with a hydrophilic electron-withdrawing carboxylic group, for example, **18**, have higher activities than those with hydrophobic electron-donating methoxy group, for example, **17**, and the hydrophobic electron-donating methyl group, **16**, against both HepG2 and HCT-116, respectively. However, the more hydrophobic electron-donating methoxy group, for example, **17**, and the hydrophobic electron-donating methyl group, **16**, exhibited higher activities than the hydrophilic electron-withdrawing carboxylic group, for example, **18**, against MCF-7 cell line, respectively. Compounds with substitutions at the phenyl tail, for example, **18**, **17**, and **16**, displayed higher activities than the unsubstituted one, for example, **15**, against HepG2, HCT-116, and MCF-7 cell lines. Furthermore, the terminal pyridine tail, as in compound **19**, exhibited higher activities than the phenyl tail **15** against HepG2, HCT-116, and MCF-7 cell lines, respectively.

Moreover, the dichloro derivatives with unsubstituted phenyl group **15** and with 4-methylphenyl group **16** exhibited higher anticancer activities than the monochloro derivatives **7** and **8** against both HepG2 and MCF-7 cell lines, respectively, but they displayed lower activity against HCT-116 cell line, respectively. Furthermore, the dichloro derivative with 4-carboxylicphenyl group **18** exhibited higher anticancer activities than the monochloro derivative **10** against HepG2, HCT-116, and MCF-7 cell lines, respectively.

In addition, the amide derivatives **7**–**14** in series 2 displayed higher activities than the ester derivatives **4**–**6** in series 1 against HepG2, HCT-116, and MCF-7 cell lines.

The data obtained from VEGFR-2 inhibition assay concluded that generally compounds with 2,4-dichlorobenzylidene moiety, for example, **15**, **16**, and **18**, exhibited higher VEGFR-2 inhibition activities than that with 4-chlorobenzylidene moiety, for example, **7**, **8**, and **10**, respectively. The phenyl tail substituted with hydrophilic electron-withdrawing carboxylic and aminocarbonyl groups, either in

2,4-dichlorobenzylidene and/or 4-chlorobenzylidene derivatives, as in compounds **18**, **11**, and **10** respectively, displayed the highest activities at IC_{50} values of 0.26 ± 0.03, 0.28 ± 0.03, and 0.29 ± 0.03 μM, respectively. In 4-chlorobenzylidene derivatives, compounds with acetyl substituent **9** showed higher activities than that with methyl **8**, pyridine **13**, unsubstituted one **7**, nitro substituent **12**, and thiazole hetero ring **14**, respectively. Furthermore, in 2,4-dichlorobenzylidene derivatives, compounds with methoxy substituent, for example, **17**, displayed a higher activity than methyl **16**, heteroaromatic pyridine **19**, and the unsubstituted phenyl **15**, respectively.

2.6 | Absorption, distribution, metabolism, excretion, and toxicity (ADMET) profiling study

In this study, an in silico analysis of the three most active compounds (**18**, **11**, and **10**) was conducted to evaluate their physicochemical properties and the suggested ADMET profiles. This study was conducted with the aid of pkCSM descriptors algorithm protocol[60] and according to the directions of Lipinski's rule.[61] A compound is expected to have good absorption properties if the molecule conforms to at least three of Lipinski's rules: (i) HBD groups ≤5; (ii) HBA groups ≤10; (iii) molecular weight <500; (iv) log *P* < 5. In the present work, reference anticancer agents sorafenib and doxorubicin were found to violate three and one of Lipinski's rules, respectively. Gratifyingly, new compounds constructed in this study do not violate any of Lipinski's rules. Whereas the molecular weight of doxorubicin exceeded the specified limit by 43 atomic mass units (amu), our newly designed ligands were below the limit by more than 50 amu. Also, sorafenib, the standard VEGFR-2 degrader, violated the optimum log *P* value, whereas new ligands did not. All the three active derivatives have five HBA groups and a number of HBD groups between 2 and 3, and these values are in line with Lipinski's rules. ADMET profiles of these three new TZDs were tentatively evaluated to examine their potentials of building up as good drug candidates.

From the obtained results (Table 2), we can conclude that these three derivatives have an intestinal absorptivity in humans (58.6–77.9) that is comparable to that of sorafenib (62.3) and better than the intestinal absorptivity of doxorubicin (62.3–84.7). This preferred property would make the new compounds easier to go along various biological membranes.[62] Therefore, they may have a considerable good bioavailability after oral administration. Regarding the central nervous system (CNS) permeability, our synthesized thiazolidinediones **18**, **11**, and **10** demonstrated an equivalent ability as sorafenib to penetrate the CNS (CNS permeability values approximately −2.2), whereas the standard anticancer agent doxorubicin was unable to penetrate (CNS permeability < −4.0).

It is also obvious that cytochrome P3A4, the major enzyme included in the metabolism of drug, could be inhibited by the effect of sorafenib, whereas doxorubicin and new ligands could not inhibit it. Excretion was predicted on the basis of the total clearance, which is a considerable parameter in determining dose intervals. Tabulated data revealed that sorafenib and doxorubicin revealed higher total clearance values as compared with new ligands. Thus, sorafenib and doxorubicin could be excreted faster, and are consequently expected to have shorter dosing intervals. Unlike sorafenib and doxorubicin, compounds **18**, **11**, and **10** displayed a slower clearance rate, which reflects the preference of possible prolonged dosing intervals. The last studied parameter in the ADMET profiles of our synthesized VEGFR-2 inhibitors is toxicity. As presented in Table 2, sorafenib, doxorubicin, and all the new compounds shared the disadvantage of undesirable hepatotoxic effects. Unlike the carboxamide derivative **11**, sorafenib and doxorubicin, **10**, and **18** showed the preference of higher maximum tolerated dose, which means the advantage of the narrow therapeutic index of the former and the wide therapeutic index of **10** and **18**. The oral acute toxic doses of the new compounds (LD_{50}) are roughly the same as for the reference drugs (~2.50 for new thiazolidine-diones compared with 2.50 of sorafenib and 2.40 of doxorubicin). Finally, the lower Minnow toxicity values of the new derivatives as compared with doxorubicin reflect the higher selectivity of **18**, **11**, and **10** against cancer cells over their cytotoxicity against normal cells.

2.7 | Docking studies

In the present work, all modeling experiments were performed using Molsoft software. Each experiment used VEGFR-2 downloaded from the Brookhaven Protein Databank (PDB ID: 3B8Q).[63]

The obtained results indicated that all studied ligands have a similar position and orientation inside the recognized binding site of VEGFR-2, which reveals a large space bounded by a membrane-binding domain that serves as an entry channel for the substrate to the active site (Figure 6). In addition, the affinity of any small molecule can be considered as a unique tool in the field of drug design. There is a relationship between the affinity of organic molecules and the free binding energy.[49,64–66] This relationship can contribute to the prediction and interpretation of the activity of the organic compounds toward the specific target protein. The obtained results of the free energy of binding (Δ*G*) explained that most of these compounds had a good binding affinity toward the receptor, and the computed values reflected the overall trend (Table 3).

The proposed binding mode of sorafenib revealed an affinity value of −94.12 kcal/mol and four H-bonds. The *N*-methylpicolinamide moiety was stabilized by the formation of two H-bonds with the essential amino acid Cys919, where the pyridine N atom formed one H-bond with the NH of Cys919 (2.94 Å), whereas its NH group formed one H-bond with the carbonyl of Cys919 (2.07 Å). The urea linker formed one H-bond with the key amino acid Glu885 (2.40 Å) through its NH group and one H-bond with Asp1046 (2.08 Å) through its carbonyl group. The *N*-methylpicolinamide moiety occupied the hydrophobic ATP-binding pocket formed by Leu1035, Lys920, Cys919, Phe918, Glu917, Val848, and Leu840. Moreover, the central phenyl ring occupied the hydrophobic pocket formed by Cys1045, Leu1035, Thr916, Lys868, and Val848. Furthermore, the hydrophobic 3-trifluromethyl-4-chlorophenyl moiety attached to the urea linker

TABLE 2 ADMET profile of the three most active compounds, sorafenib, and doxorubicin

Parameters	10	11	18	Sorafenib	Doxorubicin
Molecular properties					
Molecular weight	416.842	415.858	451.287	464.831	543.525
Log *P*	3.7132	3.1139	4.3666	5.5497	0.0013
H-acceptors	5	5	5	4	12
H-donors	2	2	2	3	6
Surface area	168.524	169.070	178.827	185.111	222.081
Absorption					
Water solubility	−4.219	−4.51	−4.312	−4.888	−2.915
Caco2 permeability	1.016	0.975	0.786	0.613	0.457
Intestinal abs. in human	58.617	77.939	59.796	84.731	62.372
Skin permeability	−2.735	−2.854	−2.735	−2.776	−2.735
P-glycoprotein substrate	Yes	Yes	Yes	Yes	Yes
P-glycoprotein I inhibitor	No	Yes	No	Yes	No
Distribution					
VDss (human)	−1.247	−0.246	−1.173	−0.233	1.647
BBB permeability	−1.321	−1.129	−1.472	−1.682	−1.379
CNS permeability	−2.315	−2.412	−2.197	−1.995	−4.307
Metabolism					
CYP3A4 substrate	No	No	No	Yes	No
CYP1A2 inhibitor	No	No	No	Yes	No
CYP3A4 inhibitor	No	No	No	Yes	No
Excretion					
Total clearance	−0.279	−0.488	−0.29	−0.212	0.987
Renal OCT2 substrate	No	No	No	No	No
Toxicity					
Max. tolerated dose (human)	0.022	−0.389	0.135	0.677	0.081
Oral rat acute toxicity (LD_{50})	2.595	2.312	2.684	2.595	2.408
Hepatotoxicity	Yes	Yes	Yes	Yes	Yes
Skin sensitization	No	No	No	No	No
Minnow toxicity	1.022	1.153	0.343	−0.421	4.412

Abbreviations: BBB, blood–brain barrier; CNS, central nervous system; VDss, steady-state volume of distribution.

occupied the hydrophobic pocket formed by Asp1046, Cys1045, Hie1026, Ile892, Ile888, and Glu885 (Figure 7). The urea linker played an important role in the binding affinity toward VEGFR-2 enzyme, where it was responsible for the higher binding affinity of sorafenib. These findings encourage us to use acetamide linkers resembling urea of sorafenib, hoping to obtain potent VEGFR-2 inhibitors.

As planned, the proposed binding mode of compound **18** is virtually the same as that of sorafenib, which revealed an affinity value of −94.02 kcal/mol and four H-bonds. The carboxylic group was stabilized by the formation of two H-bonds with Cys919, the essential amino acid in ATP-binding site, with distances of 1.35 and 2.72 Å. The NH group of the acetamide linker formed one H-bond with Thr916 (2.46 Å). Moreover, the carbonyl group at position 2 of TZD formed one H-bond with Asp1044 (2.58 Å). The 2,4-dichlorophenyl moiety occupied the hydrophobic groove formed by Asp1046, Cys1045, Hie1026, Ile892, Ile888, and Glu885. Moreover, the TZD moiety occupied the hydrophobic pocket formed by Asp1046, Cys1045, Glu885, and Lys868. The 4-carboxylicphenyl moiety occupied the hydrophobic ATP-binding pocket formed by Leu1035, Lys920, Cys919, Phe918, Glu917, Thr916, Val848, and Leu840 (Figure 8).

The proposed binding mode of compound **11** is virtually the same as that of sorafenib and **18**, which revealed an affinity value of

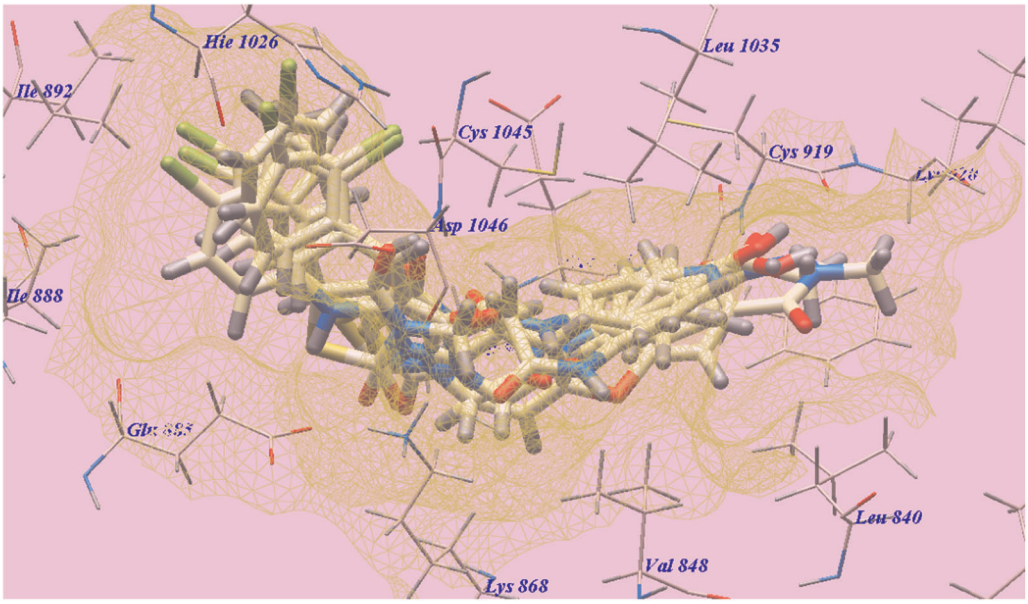

FIGURE 6 Superimposition of some docked compounds inside the binding pocket of 3B8Q

−82.30 kcal/mol and four H-bonds. The carboxamide group was stabilized by the formation of two H-bonds with the essential amino acid Cys919 (1.37 and 2.09 Å). The carbonyl group of the acetamide linker formed one H-bond with Asp1044 (2.96 Å). Moreover, the carbonyl group at position 2 of TZD formed another H-bond with Asp1044 (1.68 Å). The 4-chlorophenyl moiety occupied the hydrophobic groove formed by Asp1046, Cys1045, Hie1026, Ile892, Ile888, and Glu885. Moreover, the TZD moiety occupied the hydrophobic pocket formed by Asp1046, Cys1045, Glu885, and Lys868. The 4-carboxamidephenyl moiety occupied the hydrophobic ATP-binding pocket formed by Leu1035, Lys920, Cys919, Phe918, Glu917, Thr916, Val848, and Leu840 (Figure 9).

The proposed binding mode of compound **10** is virtually the same as that of sorafenib and **18**, which revealed an affinity value of −80.54 kcal/mol and four H-bonds. The carboxylic group was stabilized by the formation of two H-bonds with the essential amino acid Cys919 (1.65 and 1.91 Å). The carbonyl group of the acetamide linker formed one H-bond with Lys868 (2.24 Å). Moreover, the carbonyl group at position 2 of TZD formed one H-bond with Asp1044 (1.46 Å). The 4-chlorophenyl moiety occupied the hydrophobic groove formed by Asp1046, Cys1045, Hie1026, Ile892, Ile888, and Glu885. Moreover, the TZD moiety occupied the hydrophobic pocket formed by Asp1046, Cys1045, Glu885, and Lys868. The 4-carboxylicphenyl moiety occupied the hydrophobic ATP-binding pocket formed by Leu1035, Lys920, Cys919, Phe918, Glu917, Thr916, Val848, and Leu840 (Figure 10).

TABLE 3 The calculated ΔG (free energy of binding) and binding affinities for the ligands

Compound	ΔG (kcal/mol)	Compound	ΔG (kcal/mol)
4	−57.63	**13**	−64.34
5	−60.27	**14**	−58.39
6	−60.49	**15**	−68.24
7	−62.99	**16**	−72.54
8	−69.89	**17**	−79.09
9	−73.76	**18**	−94.02
10	−80.54	**19**	−67.84
11	−82.30	Sorafenib	−94.12
12	−62.53		

The proposed binding mode of compound **17** is virtually the same as that of sorafenib and **18**, which revealed an affinity value of −79.09 kcal/mol and three H-bonds. The methoxy group formed one H-bond through its oxygen atom with the essential amino acid Cys919 (2.03 Å). The NH group of the acetamide linker formed one H-bond with Thr916 (2.72 Å). Moreover, the carbonyl group at position 2 of TZD formed one H-bond with Asp1044 (2.58 Å). The 2,4-dichlorophenyl moiety occupied the hydrophobic groove formed by Asp1046, Cys1045, Hie1026, Ile892, Ile888, and Glu885. Moreover, the TZD moiety occupied the hydrophobic pocket formed by Asp1046, Cys1045, Glu885, and Lys868. The 4-methoxyphenyl moiety occupied the hydrophobic ATP-binding pocket formed by Leu1035, Lys920, Cys919, Phe918, Glu917, Thr916, Val848, and Leu840 (Figure 11).

From the obtained docking results (Table 3), we concluded that the acetamide linker played an important role in increasing the affinity toward the VEGFR-2 enzyme. The lipophilicity of the 2,4-dichlorobenzylidene and 4-chlorobenzylidene moieties played an important role in the hydrophobic interactions and, consequently, in increasing affinities toward VEGFR-2 enzyme. The TZD enables the new compounds to form H-bonds through its carbonyl group at position 2 with the amino acid residue Asp1046. Furthermore, the heteroaromatic rings and/or the substituted phenyl groups with hydrophilic

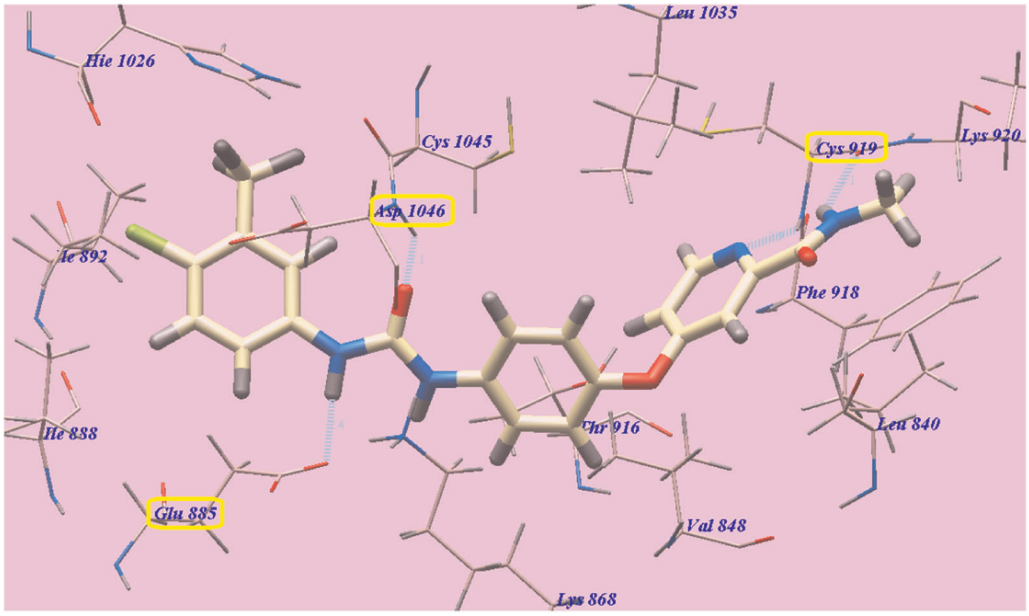

FIGURE 7 The predicted binding mode of sorafenib with VEGFR-2. H-bonded atoms are indicated by dotted lines

moieties such as carboxylic and or carboxamide groups are necessary for activity, because the NH groups and/or O atoms as the HBD–HBA motif contribute hydrogen-bonding interactions with carbonyl and NH groups of the essential amino acid Cys919 in the adenine-binding site of the receptor.

3 | CONCLUSION

The molecular design was performed to investigate the binding mode of the proposed compounds with VEGFR-2 receptor. The data obtained from the docking studies were highly correlated with that obtained from the biological screening. All the tested compounds showed variable anticancer activities. A novel series of 5-(4-chlorobenzylidene)-thiazolidine-2,4-dione derivatives **4**–**14** and 5-(2,4-dichlorobenzylidene)thiazolidine-2,4-dione derivatives **15**–**19** was designed, synthesized, and evaluated for their anticancer activity against three human tumor cell lines, HCC (HepG2), colorectal carcinoma (HCT-116), and breast cancer (MCF-7) cell lines, targeting VEGFR-2 enzyme. All the tested compounds showed variable anticancer activities. HCT-116 was the most sensitive cell line to the influence of the new derivatives. In particular, compounds **18**, **11**, and **10** were found to be the most potent derivatives among all the tested compounds

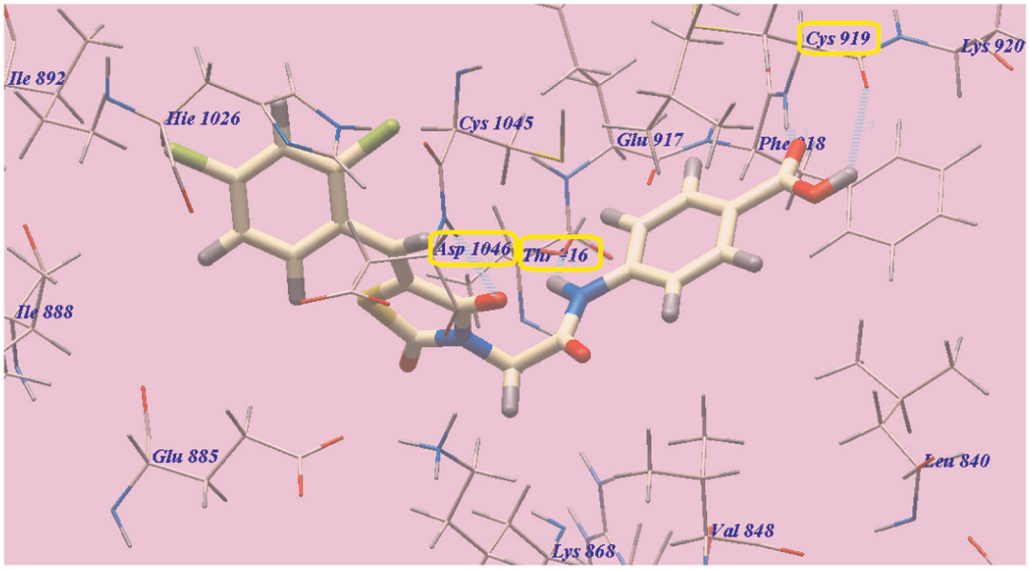

FIGURE 8 The predicted binding mode of **18** with 3B8Q

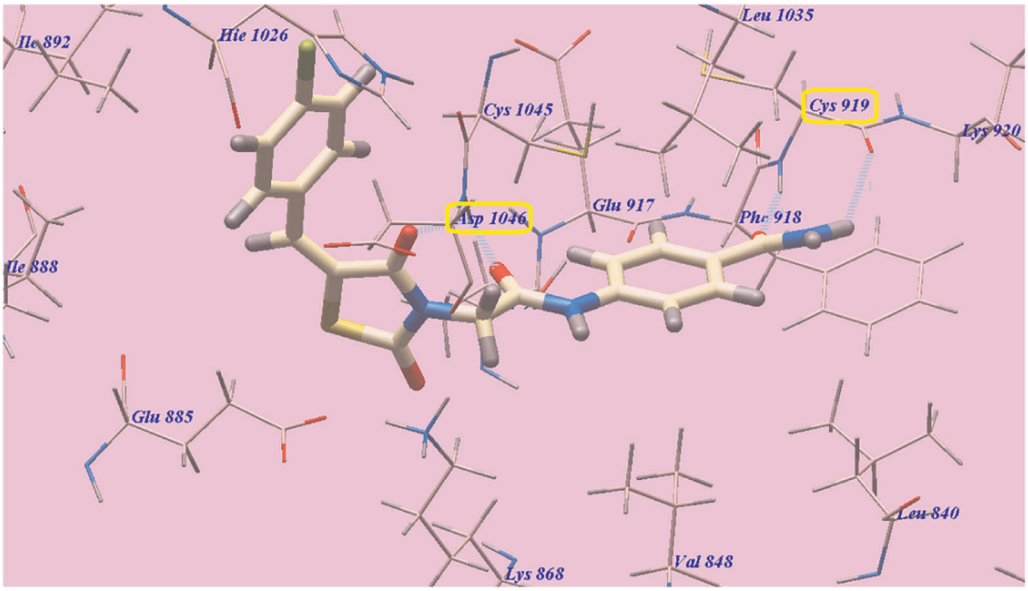

FIGURE 9 The predicted binding mode of **11** with 3B8Q

against HepG2, HCT-116, and MCF-7 cancer cell lines. The most active antiproliferative derivatives **7**–**19** were selected to evaluate their inhibitory activities against VEGFR-2. The tested compounds displayed good-to-moderate inhibitory activities. Among them, compounds **18**, **11**, and **10** were found to be the most potent VEGFR-2 inhibitors. Also, compounds **17**, **9**, and **16** possessed good VEGFR-2 inhibition. However, other compounds possessed moderate VEGFR-2 inhibition effects. Furthermore, ADMET profile was calculated for the three most active compounds, **18**, **11**, and **10**, as compared with sorafenib and doxorubicin as reference drugs. Compounds **18**, **11**, and **10** did not violate any of Lipinski's rules and had an intestinal absorptivity in humans (58.6–77.9) that is comparable to that of sorafenib (62.3) and better than the intestinal absorptivity of doxorubicin (62.3–84.7). Also, the new derivatives could not inhibit cytochrome P3A4. Unlike sorafenib and doxorubicin, compounds **18**, **11**, and **10** displayed a slower clearance rate, which reflects the preference of possible prolonged dosing intervals. Moreover, compounds **10** and **18** displayed a wide therapeutic index. Finally, the lower Minnow toxicity values of the new derivatives as compared with doxorubicin reflect the higher selectivity of **18**, **11**, and **10** against cancer cells over their cytotoxicity against normal cells.

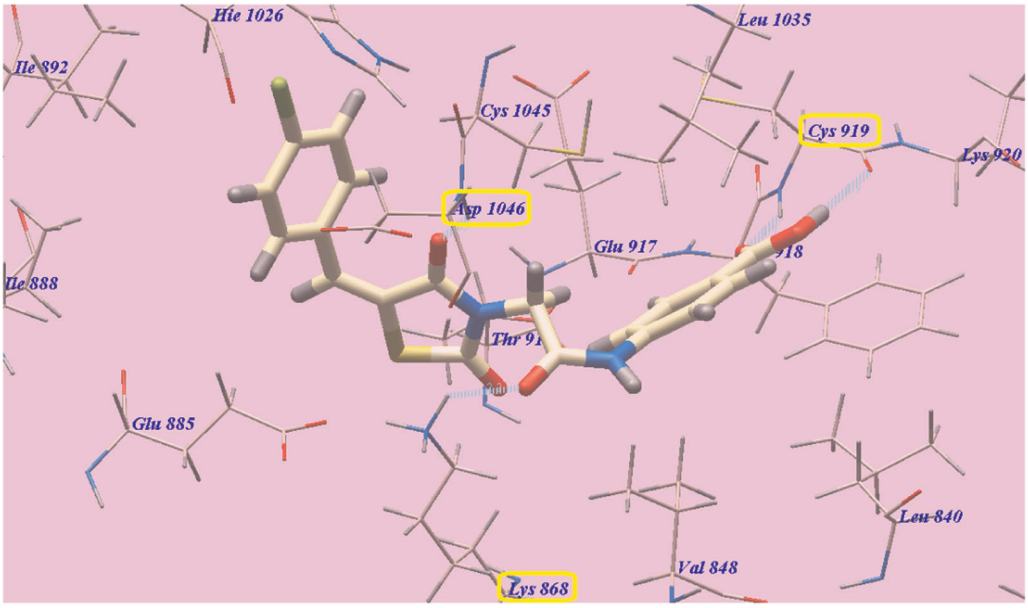

FIGURE 10 The predicted binding mode of **10** with 3B8Q

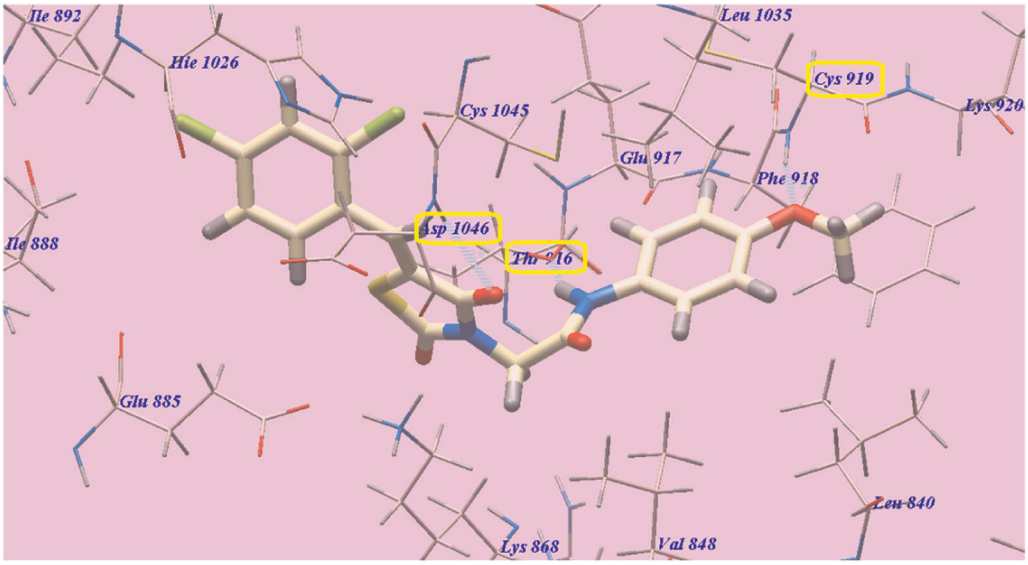

FIGURE 11 The predicted binding mode of **17** with 3B8Q

4 | EXPERIMENTAL

4.1 | Chemistry

4.1.1 | General

All melting points were determined by the open capillary method on a Gallenkamp melting point apparatus at the Faculty of Pharmacy, Al-Azhar University, and were uncorrected. The IR spectra were recorded on a Pye Unicam SP 1000 IR spectrophotometer at Microanalytical Unit, Faculty of Pharmacy, Cairo University, using the potassium bromide disc technique. ^{1}H NMR spectra were recorded on a Bruker 400 MHz-NMR spectrophotometer at the Microanalytical Unit, Faculty of Pharmacy, Cairo University. ^{13}C NMR spectra were recorded on a Bruker 100 MHz-NMR spectrophotometer at the Microanalytical Unit, Faculty of Pharmacy, Cairo University. Tetramethylsilane was used as the internal standard and chemical shifts were measured in δ scale (ppm). The mass spectra were carried out on the direct probe controller inlet part of a single-quadrupole mass analyzer in Thermo Scientific GCMS model ISQ LT, using Thermo X-Calibur software at the Regional Center for Mycology and Biotechnology, Al-Azhar University. Elemental analyses (C, H, N) were performed on a CHN analyzer at Regional Center for Mycology and Biotechnology, Al-Azhar University. All compounds were within ±0.4 of the theoretical values. The reactions were monitored by TLC using TLC sheets precoated with UV fluorescent silica gel Merck 60 F254 plates and were visualized using a UV lamp and different solvents as mobile phases.

The original spectra of the investigated compounds are provided as Supporting Information. The InChI codes of the investigated compounds, together with some biological activity data, are also provided as Supporting Information.

TZD (**1**), 5-(4-chlorobenzylidene)thiazolidine-2,4-dione and 5-(2,4-dichlorobenzylidene)thiazolidine-2,4-dione (**2$_{a,b}$**), the corresponding potassium salts (**3$_{a,b}$**), and *N*-aryl-2-chloroacetamide derivatives were obtained according to the reported procedure.[12,13]

4.1.2 | General method for the synthesis of alkyl 2-[5-(4-chlorobenzylidene)-2,4-dioxothiazolidin-3-yl]-acetate (**4** and/or **5**) and ethyl 2-[5-(4-chlorobenzylidene)-2,4-dioxothiazolidin-3-yl]-propanoate (**6**)

Equimolar quantities of the potassium salt **3$_a$** (2.76 g, 0.01 mol) and the appropriate α-chloroester derivative (0.01 mol), namely methyl chloroacetate, ethyl chloroacetate, and ethyl 2-chloropropanoate, in dimethylformamide (DMF) (20 ml) were heated on a water bath for 5 h in the presence of K_2CO_3 (1.38 g, 0.01 mol). The reaction mixture was poured into ice water (200 ml) and stirred for 30 min. The obtained solid was filtered and crystallized from ethanol to give the target compounds **4**–**6**, respectively.

Methyl 2-[5-(4-chlorobenzylidene)-2,4-dioxothiazolidin-3-yl]-acetate (4)

Yield, 90%; m.p. 110–112°C; IR$_{\nu max}$ (cm^{-1}): 3089 (CH aromatic), 2948 (CH aliphatic), 1741, 1681 (3C=O); ^{1}H NMR (400 MHz, dimethyl sulfoxide [DMSO]-d_6): 3.69 (s, 3H, OCH_3), 4.53 (s, 2H, CH_2), 7.64 (d, 2H, Ar–H, H-3 and H-5 of –C_6H_4, J = 8.8), 7.70 (d, 2H, Ar–H, H-2, and H-6 of –C_6H_4, J = 8.4), 8.03 (s, 1H, C=C**H**–Ph); anal. calcd. for $C_{13}H_{10}ClNO_4S$ (311.74): C, 50.09; H, 3.23; N, 4.49. Found: C, 50.21; H, 3.40; N, 4.26.

Ethyl 2-[5-(4-chlorobenzylidene)-2,4-dioxothiazolidin-3-yl]-acetate (5)

Yield, 85%; m.p. 125–126°C; IR$_{\nu max}$ (cm^{-1}): 3090 (CH aromatic), 2951 (CH aliphatic), 1743, 1681 (3C=O); ^{1}H NMR (400 MHz, DMSO-d_6): 1.22 (t, 3H, –OCH_2CH_3, J = 6.0), 4.17 (q, 2H, –OCH_2CH_3, J = 6.8),

4.51 (s, 2H, CH_2), 7.63 (d, 2H, Ar–H, H-3, and H-5 of –C_6H_4, J = 7.2), 7.69 (d, 2H, Ar–H, H-2, and H-6 of –C_6H_4, J = 8.8), 8.01 (s, 1H, C=**H**–Ph); anal. calcd. for $C_{14}H_{12}ClNO_4S$ (325.76): C, 51.62; H, 3.71; N, 4.30. Found: C, 51.88; H, 3.84; N, 4.57.

*Ethyl 2-[5-(4-chlorobenzylidene)-2,4-dioxothiazolidin-3-yl]-propanoate (**6**)*

Yield, 81%; m.p. 133–135°C; $IR_{\nu max}$ (cm^{-1}): 3090 (CH aromatic), 2912 (CH aliphatic), 1735, 1693 (3C=O); ^{1}H NMR (400 MHz, DMSO-d_6): 1.16 (t, 3H, –$OCH_2C\mathbf{H_3}$, J = 7.2), 1.52 (d, 3H, –$CHC\mathbf{H_3}$, J = 7.2), 4.14 (q, 2H, –$OC\mathbf{H_2}CH_3$, J = 7.6), 5.11 (q, 1H, –$C\mathbf{H}CH_3$, J = 7.6), 7.63 (d, 2H, Ar–H, H-3, and H-5 of –C_6H_4, J = 8.8), 7.68 (d, 2H, Ar–H, H-2, and H-6 of –C_6H_4, J = 8.4), 7.98 (s, 1H, C=C**H**–Ph); mass spectroscopy (MS) (m/z): 342.08 (M^++2, 1.51%), 341.07 (M^++1, 7.30%), 339.96 (M^+, 19.33%), 338.98 (87.24%), 133.97 (100%, base beak), 120.92 (35.83%); anal. calcd. for $C_{15}H_{14}ClNO_4S$ (339.79): C, 53.02; H, 4.15; N, 4.12. Found: C, 53.29; H, 4.37; N, 4.25.

4.1.3 | General method for the synthesis of 2-[5-(4-chlorobenzylidene)-2,4-dioxothiazolidin-3-yl]-*N*-[(un)substituted aryl]acetamide (**7**–**14**)

Equimolar quantities of the potassium salt $\mathbf{3_a}$ (2.76 g, 0.01 mol) and the appropriate *N*-aryl-2-chloroacetamide derivative (0.01 mol) in dry DMF (20 ml) were heated on a water bath for 4 h in the presence of K_2CO_3 (1.38 g, 0.01 mol). After cooling to room temperature, the reaction mixture was poured over crushed ice. The precipitated solids were filtered, dried, and crystallized from ethanol to give the corresponding target compounds **7**–**14**, respectively.

*2-[5-(4-Chlorobenzylidene)-2,4-dioxothiazolidin-3-yl]-N-phenylacetamide (**7**)*

Yield, 70%; m.p. 150–151°C; $IR_{\nu max}$ (cm^{-1}): 3275 (NH), 3059 (CH aromatic), 2924 (CH aliphatic), 1694, 1657, 1636 (3C=O); ^{1}H NMR (400 MHz, DMSO-d_6): 4.53 (s, 2H, –CH_2), 7.08 (m, 1H, Ar–H, H-4 of –C_6H_5), 7.35 (m, 2H, Ar–H, H-3, and H-5 of –C_6H_5), 7.55 (m, 4H, Ar–H, H–4, and H-6 of –C_6H_5 and Ar–H, H-3, and H-5 of C_6H_4Cl), 7.68 (m, 2H, Ar–H, H-3, and H-6 of C_6H_4Cl), 8.01 (s, 1H, C=C**H**–Ph), 10.41 (s, 1H, NH, D_2O exchangeable); ^{13}C NMR (100 MHz, DMSO-d_6): 44.55, 119.64 (2), 122.21, 124.21, 129.36 (2), 129.97 (2), 132.23 (2), 132.31, 132.78, 135.91, 138.83, 164.19, 165.67, 167.36; anal. calcd. for $C_{18}H_{13}ClN_2O_3S$ (372.83): C, 57.99; H, 3.51; N, 7.51. Found: C, 58.26; H, 3.68; N, 7.75.

*2-[5-(4-Chlorobenzylidene)-2,4-dioxothiazolidin-3-yl]-N-(p-tolyl)-acetamide (**8**)*

Yield, 70%; m.p. 155–157°C; $IR_{\nu max}$ (cm^{-1}): 3278 (NH), 3066 (CH aromatic), 2850 (CH aliphatic), 1751, 1693 (3C=O); ^{1}H NMR (400 MHz, DMSO-d_6): 2.26 (s, 3H, –CH_3), 4.49 (s, 2H, –CH_2), 7.12 (d, 2H, Ar–H, H-3, and H-5 of –C_6H_4–CH_3, J = 8.0), 7.42 (d, 2H, Ar–H, H-2, and H-6 of –C_6H_4–CH_3, J = 6.4), 7.52 (d, 2H, Ar–H, H-3, and H-5 of –C_6H_4–Cl, J = 6.0), 7.69 (d, 2H, Ar–H, H-2, and H-6 of –C_6H_4Cl, J = 8.0), 8.01 (s, 1H, C=CH–Ph), 10.32 (s, 1H, NH, D_2O exchangeable); anal. calcd. for $C_{19}H_{15}ClN_2O_3S$ (386.85): C, 58.99; H, 3.91; N, 7.24. Found: C, 59.17; H, 4.06; N, 7.40.

N-*(4-Acetylphenyl)-2-[5-(4-chlorobenzylidene)-2,4-dioxothiazolidin-3-yl]acetamide (**9**)*

Yield, 60%; m.p. 153–155°C; $IR_{\nu max}$ (cm^{-1}): 3277 (NH), 3062 (CH aromatic), 2855 (CH aliphatic), 1755, 1693 (4C=O); ^{1}H NMR (400 MHz, DMSO-d_6): 2.52 (s, 3H, $COCH_3$), 4.58 (s, 2H, CH_2), 7.56 (d, 2H, Ar–H, H-3, and H-5 of –C_6H_4Cl), 7.62 (d, 2H, Ar–H, H-2, and H-6 of –C_6H_4Cl), 7.71 (d, 2H, Ar–H, H-2, and H-6 of –$C_6H_4COCH_3$), 7.96 (d, 2H, Ar–H, H-3, and H-5 of –$C_6H_4COCH_3$), 7.98 (s, 1H, C=C**H**–Ph), 10.45 (s, 1H, NH, D_2O exchangeable); ^{13}C NMR (100 MHz, DMSO-d_6): 34.58, 38.52, 118.91 (2), 122.63, 129.93 (3), 130.77 (2), 131.94, 132.21 (3), 132.35, 135.69, 143.18, 165.83, 167.36, 169.30; anal. calcd. for $C_{20}H_{15}ClN_2O_4S$ (414.86): C, 57.90; H, 3.64; N, 6.75. Found: C, 58.16; H, 3.75; N, 6.93.

*4-{2-[5-(4-Chlorobenzylidene)-2,4-dioxothiazolidin-3-yl]acetamido}-benzoic acid (**10**)*

Yield, 73%; m.p. 167–169°C; $IR_{\nu max}$ (cm^{-1}): 3417 (OH), 3232 (NH), 3012 (CH aromatic), 2839 (CH aliphatic), 1735, 1685 (4C=O); ^{1}H NMR (400 MHz, DMSO-d_6): δ = 4.72 (s, 2H, CH_2), 7.07 (s, 1H, C=C**H**–Ph), 7.42–7.67 (m, 2H, Ar–H, H-2, and H-6 of –C_6H_4–Cl), 7.66–7.73 (m, 2H, H-3, and H-5 of C_6H_4–Cl), 7.75–7.88 (m, 2H, Ar–H, H-2, and H-6 of C_6H_4–COOH), 7.90–8.26 (m, 2H, Ar–H, H-3, and H-5 of C_6H_4–COOH), 11.31 (s, 1H, NH, D_2O exchangeable), 12.53 (s, 1H, –OH, D_2O exchangeable); ^{13}C NMR (100 MHz, DMSO-d_6): 36.42, 125.55, 129.80 (3), 130.34 (2), 132.02 (3), 132.56 (2), 135.29 (2), 168.56 (2), 173.57, 174.34; MS (m/z): 416 (M^+, 15.75%), 246 (10.34%), 78 (100%, base beak), 71 (23.12%); anal. calcd. for $C_{19}H_{13}ClN_2O_5S$ (416.83): C, 54.75; H, 3.14; N, 6.72. Found: 54.97; H, 3.42; N, 6.83.

*4-{2-[5-(4-Chlorobenzylidene)-2,4-dioxothiazolidin-3-yl]acetamido}-benzamide (**11**)*

Yield, 92%; m.p. 190–192°C; $IR_{\nu max}$ (cm^{-1}): 3282 (NH), 3066 (CH aromatic), 2843 (CH aliphatic), 1739, 1681 (4C=O); ^{1}H NMR (400 MHz, DMSO-d_6): 3.98 (s, 2H, CH_2), 7.25 (s, 2H, NH_2) (D_2O exchangeable), 7.63–7.65 (m, 4H, Ar–H, H-2, H-3, H-5, and H-6 of –C_6H_4Cl), 7.72–7.75 (m, 4H, Ar–H, H-2, H-3, H-5, and H-6 of benzamide), 7.94 (s, 1H, C=CH-Ph), 10.40 (s, H, NH) (D_2O exchangeable); ^{13}C NMR (100 MHz, DMSO-d_6): 44.57, 119.59 (2), 122.18, 129.09, 129.67 (2), 130.22 (2), 130.35 (3), 131.17, 133.04, 136.47, 140.54, 152.92, 164.62, 166.46; MS (m/z): 416.98 (M^++2, 9.67%), 415 (M^+, 25.44%), 338.06 (100%, base beak), 305.65 (58.57%), 236.23 (43.73%), 71.19 (15.14%); anal. calcd. for $C_{19}H_{14}ClN_3O_4S$ (415.85): C, 54.88; H, 3.39; N, 10.10. Found: C, 54.71; H, 3.70; N, 10.34.

*2-[5-(4-Chlorobenzylidene)-2,4-dioxothiazolidin-3-yl]-N-(4-nitrophenyl)acetamide (**12**)*

Yield, 68%; m.p. 180–182°C; $IR_{\nu max}$ (cm^{-1}): 3259 (NH), 3065 (CH aromatic), 2852 (CH aliphatic), 1754, 1693 (3C=O); ^{1}H NMR

(400 MHz, DMSO-d_6): 4.61 (s, 2H, CH_2), 7.64 (d, 2H, Ar–H, H-3, and H-5 of –C_6H_4Cl, J = 6.8), 7.70 (d, 2H, Ar–H, H-2, and H-6 of –C_6H_4Cl, J = 8.4), 7.82 (d, 2H, Ar–H, H-2, and H-6 of –C_6H_4–NO_2, J = 10.0), 8.00 (s, 1H, C═C**H**–Ph), 8.25 (d, 2H, Ar–H, H-3, and H-5 of –C_6H_4–NO_2, J = 8.0), 11.04 (s, 1H, NH, D_2O exchangeable); anal. calcd. for $C_{18}H_{12}ClN_3O_5S$ (417.82): C, 51.74; H, 2.90; N, 10.06. Found: C, 51.91; H, 3.11; N, 10.35.

*2-[5-(4-Chlorobenzylidene)-2,4-dioxothiazolidin-3-yl]-N-(pyridin-2-yl)acetamide (**13**)*

Yield, 68%; m.p. 182–184°C; $IR_{\nu max}$ (cm^{-1}): 3151 (NH), 3051 (CH aromatic), 2765 (CH aliphatic), 1755, 1678 (3C═O); ^1H NMR (400 MHz, DMSO-d_6): 4.61 (s, 2H, CH_2), 7.15 (m, 1H, Ar–H, H-4 of pyridine), 7.53 (d, 2H, Ar–H, H-3, and H-5 of –C_6H_4Cl, J = 8.8), 7.65 (d, 2H, Ar–H, H-2, and H-6 of –C_6H_4Cl, J = 10.8), 7.82 (m, 1H, Ar–H, H-5 of pyridine), 7.98 (s, 1H, C═C**H**–Ph), 8.00 (d, 1H, Ar–H, H-6 of pyridine, J = 9.6), 8.36 (d, 1H, Ar–H, H-3 of pyridine, J = 8.4), 11.02 (s, 1H, –NH, D_2O exchangeable); ^{13}C NMR (100 MHz, DMSO-d_6): 55.95, 113.96, 115.37, 120.32, 125.79, 132.04, 132.51, 132.86, 132.96, 134.10, 138.89, 148.59, 161.79, 161.91, 165.24, 165.87, 168.67; anal. calcd. for $C_{17}H_{12}ClN_3O_3S$ (373.81): C, 54.62; H, 3.24; N, 11.24. Found: C, 54.85; H, 3.45; N, 11.47.

*2-[5-(4-Chlorobenzylidene)-2,4-dioxothiazolidin-3-yl]-N-(thiazol-2-yl)acetamide (**14**)*

Yield, 55%; m.p. 185–187°C; $IR_{\nu max}$ (cm^{-1}): 3275 (NH), 3086 (CH aromatic), 2850 (CH aliphatic), 1747, 1693 (3C═O); ^1H NMR (400 MHz, DMSO-d_6): 4.25 (s, 2H, –CH_2), 7.34 (d, 1H, Ar–H, H-5 of thiazol), 7.62 (d, 2H, Ar–H, H-3, and H-5 of –C_6H_5Cl, J = 7.6), 7.69 (d, 2H, Ar–H, H-2, and H-6 of –C_6H_5Cl, J = 8.0), 7.74 (d, 1H, Ar–H, H-4 of thiazol), 7.97 (s, 1H, –C═C**H**–Ph), 11.05 (s, 1H, NH, D_2O exchangeable); MS (*m/z*): 381.44 (M^++2, 18.26%), 380.77 (M^++1, 50.58%), 330.37 (79.85%), 293.81 (100%, base beak), 239.02 (83.26%), 71.49 (49.68%); anal. calcd. for $C_{15}H_{10}ClN_3O_3S_2$ (379.83): C, 47.43; H, 2.65; N, 11.06. Found: C, 47.69; H, 2.91; N, 11.28.

4.1.4 | General procedure for the synthesis of target compounds (**15**–**19**)

Equimolar quantities of the potassium salt **3b** (3.12 g, 0.01 mol) and the appropriate *N*-aryl-2-chloroacetamide derivative (0.01 mol) in dry DMF (20 ml) were heated on a water bath for 4 h in the presence of K_2CO_3 (1.38 g, 0.01 mol). After cooling to room temperature, the reaction mixture was poured over crushed ice. The precipitated solids were filtered, dried, and crystallized from ethanol to give the corresponding target compounds **15**–**19**, respectively.

*2-[5-(2,4-Dichlorobenzylidene)-2,4-dioxothiazolidin-3-yl]-N-phenylacetamide (**15**)*

Yield, 60%; m.p. 170–171°C; IR (KBr) ν_{max} 3294, 3063, 2932, 1701, 1667 cm^{-1}; ^1H NMR (400 MHz, DMSO-d_6): δ = 4.52 (s, 2H, –CH_2), 7.07–7.10 (m, 1H, Ar–H, H-4 of –C_6H_5), 7.30–7.35 (m, 2H, Ar–H, H-3, and H-5 of –C_6H_5), 7.55 (d, 1H, Ar–H, H-5 of –$C_6H_3(Cl_2)$, J = 9.6), 7.62–7.64 (m, 2H, Ar–H, H-2, and H-6 of –C_6H_5), 7.69–7.71 (m, 2H, Ar–H, H-3, and H-6 of –$C_6H_3(Cl_2)$), 8.00 (s, 1H, C═C**H**–Ph), 10.41 (s, 1H, NH, D_2O exchangeable); MS (*m/z*): 409.86 (M^++2, 21.87%), 407.90 (M^++1, 34.66%), 407.22 (M^+, 32.75%), 405.89 (61.28%), 373.03 (65.48%), 370.87 (100%, base beak), 93.27 (32.13%), 77.07 (50.54%); anal. calcd. for $C_{18}H_{12}Cl_2N_2O_3S$ (407.27): C, 53.09; H, 2.97; N, 6.88. Found: C, 53.13; H, 2.67; N, 6.79.

*2-[5-(2,4-Dichlorobenzylidene)-2,4-dioxothiazolidin-3-yl]-N-(p-tolyl)acetamide (**16**)*

Yield, 70%; m.p. 175–176°C; IR (KBr) ν_{max} 3202, 3067, 2932, 1697 cm^{-1}; ^1H NMR (400 MHz, DMSO-d_6): δ = 2.26 (s, 3H, –CH_3), 4.50 (s, 2H, –CH_2), 7.13 (d, 2H, Ar–H, H-3, and H-5 of –C_6H_4–CH_3, J = 6.0), 7.44 (d, 2H, Ar–H, H-2, and H-6 of –C_6H_4–CH_3, J = 6.8), 7.62–7.70 (m, 3H, Ar–H, H-3, H-5, and H-6 of –$C_6H_3(Cl_2)$), 8.01 (s, 1H, –C═C**H**–Ph), 10.33 (s, 1H, NH, D_2O exchangeable); ^{13}C NMR (100 MHz, DMSO-d_6): δ = 20.90, 44.48, 119.65 (2), 121.49, 129.72 (2), 129.90 (2), 130.67 (2), 131.29, 133.14, 133.34, 134.05, 136.36, 163.97, 165.78, 167.60; MS (*m/z*): 423.88 (M^++2, 11.97%), 422.94 (M^++1, 10.89%), 421.90 (M^+, 32.71%), 419.91 (47.52%), 373.84 (1.25%), 106.99 (51.27%), 77.04 (52.96%), 72.04 (100%, base beak); anal. calcd. for $C_{19}H_{14}Cl_2N_2O_3S$ (421.29): C, 54.17; H, 3.35; N, 6.65. Found: C, 53.96; H, 3.45; N, 6.87.

*2-[5-(2,4-Dichlorobenzylidene)-2,4-dioxothiazolidin-3-yl]-N-(4-methoxyphenyl)acetamide (**17**)*

Yield, 65%; m.p. 172–174°C; IR (KBr) ν_{max} 3333, 3036, 2924, 1705, 1663 cm^{-1}; ^1H NMR (400 MHz, DMSO-d_6): δ = 3.81 (s, 3H, OCH_3), 3.83 (s, 2H, CH_2), 7.08–7.10 (m, 4H, Ar–H, H-2, H-3, H-5, and H-6 of –$C_6H_4(OCH_3)$), 7.64–7.66 (m, 4H, Ar–H, 3H of –$C_6H_3(Cl_2)$ and 1H, C═C**H**–Ph), 11.34 (s, 1H, NH, D_2O exchangeable); ^{13}C NMR (100 MHz, DMSO-d_6): δ = 34.58, 38.52, 118.73 (2), 121.86, 129.86 (3), 130.59 (4), 131.10, 133.27, 133.44, 142.35, 165.94, 167.61, 169.14; MS (*m/z*): 439 (M^++3, 4.88%), 438 (M^++2, 14.27%), 437 (M^++1, 24.35%), 436 (M^+, 15.82%), 120 (100%, base beak), 91 (38.97%); anal. calcd. for $C_{19}H_{14}Cl_2N_2O_4S$ (436.01): C, 52.19; H, 3.23; N, 6.41. Found: 52.06; H, 3.49; N, 6.21.

*4-{2-[5-(2,4-Dichlorobenzylidene)-2,4-dioxothiazolidin-3-yl]-acetamido}benzoic acid (**18**)*

Yield, 70%; m.p. 176–178°C; IR (KBr) ν_{max} 3414, 3233, 3032, 2928, 1730, 1697 cm^{-1}; ^1H NMR (400 MHz, DMSO-d_6): δ = 4.54 (s, 2H, CH_2), 7.15 (m, H, Ar–H, H-5 of –$C_6H_3(Cl_2)$), 7.65–7.71 (m, 4H, Ar–H, H-3, and H-6 of –$C_6H_3(Cl_2)$ and H-2 and H-6 of C_6H_4–COOH), 7.78–7.84 (m, 2H, Ar–H, H-3, and H-5 of C_6H_4–COOH), 8.02 (s, 1H, C═C**H**–Ph), 10.67 (s, 1H, NH, D_2O exchangeable), 12.20 (s, 1H, –OH, D_2O exchangeable); ^{13}C NMR (100 MHz, DMSO-d_6): 44.43, 119.73, 119.96, 120.24, 127.05 (2), 130.53 (2), 130.59, 130.76, 134.12, 136.61, 141.69, 144.26, 144.44, 164.01, 164.86, 165.84, 167.64; MS (*m/z*): 454.01 (M^++3, 21.09%), 453.09 (M^++2, 23.89%), 450.75 (M^+, 29.61%), 292.20 (100%, base beak), 259.20 (82.11%), 71.36

(37.04%); anal. calcd. for $C_{19}H_{12}Cl_2N_2O_5S$ (451.27): C, 50.57; H, 2.68; N, 6.21. Found: C, 50.28; H, 3.04; N, 6.25.

*2-[5-(2,4-Dichlorobenzylidene)-2,4-dioxothiazolidin-3-yl]-N-(pyridin-2-yl)acetamide (**19**)*

Yield, 65%; m.p. 177–179°C; IR (KBr) ν_{max} 3275, 3059, 2924, 1701, 1666, 1659 cm^{-1}; ^1H NMR (400 MHz, DMSO-d_6): $\delta = 4.60$ (s, 2H, CH_2), 7.15 (m, 1H, Ar–H, H-4 of pyridine), 7.63 (d, 1H, Ar–H, H-5 of $-C_6H_5(Cl_2)$, $J = 10.4$), 7.69–7.72 (m, 2H, Ar–H, H-3, and H-6 of $-C_6H_5(Cl_2)$), 7.78 (s, 1H, C═**CH**–Ph), 7.97–8.01 (m, 2H, Ar–H, H-5, and H-6 of pyridine), 8.36 (m, 1H, Ar–H, H-3 of pyridine), 10.99 (s, 1H, NH, D_2O exchangeable); MS (*m/z*): 409.98 (M^++2, 6.78%), 408.95 (M^++1, 27.79%), 407.98 (M^+, 9.57%), 406.97 (44.69%), 371.98 (43.77%), 120.97 (55.18%), 77.98 (100%, base beak); anal. calcd. for $C_{17}H_{11}Cl_2N_3O_3S$ (408.25): C, 50.01; H, 2.72; N, 10.29. Found: C, 49.65; H, 2.34; N, 10.42.

4.2 | Docking studies

In the present work, all the target compounds were subjected to a docking study to explore their binding mode toward VEGFR-2 enzyme. All modeling experiments were performed using Molsoft program, which provides a unique set of tools for the modeling of protein/ligand interactions. It predicts how small flexible molecules such as substrates or drug candidates bind to a protein of known three-dimensional structure, represented by grid interaction potentials (http://www.molsoft.com/icm_pro.html). Each experiment used the biological target VEGFR-2 downloaded from the Brookhaven Protein Data Bank (http://www.rcsb.org/pdb/explore/explore.do?structureId=1YWN). To qualify the docking results in terms of accuracy of the predicted binding conformations in comparison with the experimental procedure, the reported VEGFR-2 inhibitor drugs vatalanib and sorafenib were used as reference ligands.

4.3 | In vitro cytotoxic activity

The cytotoxicity assays were performed at the Pharmacology & Toxicology Department, Faculty of Pharmacy, Al-Azhar University, Cairo, Egypt. Cancer cells from different cancer cell lines, HCC (HepG2), breast cancer (MCF-7), and colorectal carcinoma (HCT-116), were purchased from American Type Cell Culture Collection (ATCC) and grown in the appropriate growth medium, Roswell Park Memorial Institute medium (RPMI-1640), supplemented with 100 mg/ml of streptomycin, 100 units/ml of penicillin, and 10% of heat-inactivated fetal bovine serum in a humidified, 5% (v/v) CO_2 atmosphere at 37°C. Cytotoxicity was determined by MTT assay.

Exponentially growing cells from different cancer cell lines were trypsinized, counted, and seeded at the appropriate densities (2000–1000 cells/0.33 cm^2 well) into 96-well microtiter plates. Cells were then incubated in a humidified atmosphere at 37°C for 24 h. Then, cells were exposed to different concentrations of compounds (0.1, 10, 100, and 1000 μM) for 72 h. Next, the viability of treated cells was determined using the MTT technique[59,67] as follows: Cells were incubated with 200 μl of MTT solution/well (0.5 mg/ml) (Sigma-Aldrich) and were allowed to metabolize the dye into colored, insoluble formazan crystals for 2 h. The formazan crystals were dissolved in 200 μl/well acidified isopropanol for 30 min and covered with aluminum foil, with continuous shaking using a MaxQ 2000 plate shaker (Thermo Fisher Scientific Inc.), at room temperature. Absorbance was measured at 570 nm using a Stat Fax® 4200 Plate Reader (Awareness Technology Inc.). The cell viability was expressed as a percentage of control, and the concentration that induces 50% of maximum inhibition of cell proliferation (IC_{50}) was determined using GraphPad Prism version 5 software (GraphPad Software Inc.).[68]

4.4 | In vitro VEGFR-2 kinase assay

The kinase activity of VEGFR-2 was carried out in Pharmacology & Toxicology Department, Faculty of Pharmacy, Al-Azhar University, Cairo, Egypt, and it was measured by use of an anti-phosphotyrosine antibody with the AlphaScreen system according to manufacturer's instructions.[69,70] Enzyme reactions were performed in 50 mM Tris-HCl pH 7.5, 5 mM $MnCl_2$, 5 mM $MgCl_2$, 0.01% Tween-20, and 2 mM DTT, containing 10 μM ATP, 0.1 μg/ml biotinylated poly-GluTyr (4:1), and 0.1 nM of VEGFR-2 (Millipore). Before catalytic initiation with ATP, the tested compounds at final concentrations ranging from 0 to 300 μg/ml and enzyme were incubated for 5 min at room temperature. The reactions were quenched by the addition of 25 μl of 100 mM EDTA, 10 μg/ml AlphaScreen streptavidine donor beads, and 10 μg/ml acceptor beads in 62.5 mM HEPES pH 7.4, 250 mM NaCl, and 0.1% bovine serum albumin. The plate was incubated in the dark overnight and then read by ELISA Reader (PerkinElmer). Wells containing the substrate and the enzyme without compounds were used as the reaction control. Wells containing biotinylated poly-GluTyr (4:1) and enzyme without ATP were used as the basal control. Percent inhibition was calculated by the comparison of compounds subjected to control incubations. The concentration of the test compound causing 50% inhibition (IC_{50}) was calculated from the concentration–inhibition response curve (triplicate determinations), and the data were compared with sorafenib (Sigma-Aldrich) as the standard VEGFR-2 inhibitor.

ACKNOWLEDGMENTS

The authors extend their appreciation and gratitude to Asst. Prof. Tamer Abdel-Ghany, Pharmacology & Toxicology Department, Faculty of Pharmacy, Al-Azhar University, Cairo, Egypt, for helping in the pharmacological part.

CONFLICTS OF INTERESTS

The authors declare that there are no conflicts of interests.

ORCID

Khaled El-Adl http://orcid.org/0000-0002-8922-9770

Hamada S. Abulkhair https://orcid.org/0000-0001-6479-4573

REFERENCES

[1] H. Joshi, T. Pal, C. Ramaa, *Expert Opin. Invest. Drugs* **2014**, *23*, 501. https://doi.org/10.1517/13543784.2014.884708

[2] M. Potente, H. Gerhardt, P. Carmeliet, *Cell* **2011**, *146*, 873. https://doi.org/10.1016/j.cell.2011.08.039

[3] G. Gasparini, R. Longo, M. Toi, N. Ferrara, *Nat. Clin. Pract. Oncol.* **2005**, *2*, 562. https://doi.org/10.1038/ncponc0342

[4] A. Bishayee, A. S. Darvesh, *Curr. Cancer Drug Targets* **2012**, *12*, 1095. http://www.ncbi.nlm.nih.gov/pubmed/22873221

[5] R. S. Kerbel, *N. Engl. J. Med.* **2008**, *358*, 2039. https://doi.org/10.1056/NEJMra0706596

[6] M. Shibuya, *Genes Cancer* **2011**, *2*, 1097. https://doi.org/10.1177/1947601911423031

[7] H. C. Spangenberg, R. Thimme, H. E. Blum, *Nat. Rev. Gastroenterol. Hepatol.* **2009**, *6*, 423. https://doi.org/10.1038/nrgastro.2009.86

[8] S. Koch, S. Tugues, X. Li, L. Gualandi, L. Claesson-Welsh, *Biochem. J.* **2011**, *437*, 169. https://doi.org/10.1042/BJ20110301

[9] D. K. Shah, K. M. J. Menon, L. M. Cabrera, A. Vahratian, S. K. Kavoussi, D. I. Lebovic, *Fertil. Steril.* **2010**, *93*, 2042. https://doi.org/10.1016/j.fertnstert.2009.02.059

[10] K. El-Adl, H. Sakr, M. Nasser, M. Alswah, F. M. A. Shoman, *Arch. Pharm. (Weinheim)* **2020**, *353*, e2000079. https://doi.org/10.1002/ardp.202000079

[11] C. Nastasă, R. Tamaian, O. Oniga, B. Tiperciuc, *Medicina (Buenos Aires)* **2019**, *55*, 85. https://doi.org/10.3390/medicina55040085

[12] K. El-Adl, A.-G. A. El-Helby, H. Sakr, I. H. Eissa, S. S. A. El-Hddad, F. M. I. A. Shoman, *Bioorg. Chem.* **2020**, *102*, 104059. https://doi.org/10.1016/j.bioorg.2020.104059

[13] K. El-Adl, A.-G. A. El-Helby, H. Sakr, R. R. Ayyad, H. A. Mahdy, M. Nasser, H. S. Abulkhair, S. S. A. El-Hddad, *Arch. Pharm. (Weinheim)* **2021**, *354*, e202000279. https://doi.org/10.1002/ardp.202000279

[14] S. Takahashi, *Biol. Pharm. Bull.* **2011**, *34*, 1785. https://doi.org/10.1248/bpb.34.1785

[15] M. Yousefian, R. Ghodsi, *Arch. Pharm. (Weinheim)* **2020**, *353*, e2000022. https://doi.org/10.1002/ardp.202000022

[16] P. Wu, T. E. Nielsen, M. H. Clausen, *Trends Pharmacol. Sci.* **2015**, *36*, 422. https://doi.org/10.1016/j.tips.2015.04.005

[17] A. Pircher, W. Hilbe, I. Heidegger, J. Drevs, A. Tichelli, M. Medinger, *Int. J. Mol. Sci.* **2011**, *12*, 7077. https://doi.org/10.3390/ijms12107077

[18] M. Li, X. Yu, W. Li, T. Liu, G. Deng, W. Liu, H. Liu, F. Gao, *Oncotarget* **2018**, *9*, 152. https://doi.org/10.18632/oncotarget.22077

[19] H. Wang, B. Rao, J. Lou, J. Li, Z. Liu, A. Li, G. Cui, Z. Ren, Z. Yu, *Front. Cell. Dev. Biol.* **2020**, 8. https://doi.org/10.3389/fcell.2020.00055

[20] Y. Zhang, X. Gao, Y. Zhu, D. Kadel, H. Sun, J. Chen, Q. Luo, H. Sun, L. Yang, J. Yang, Y. Sheng, Y. Zheng, K. Zhu, Q. Dong, L. Qin, *J. Exp. Clin. Cancer Res.* **2018**, *37*, 93. https://doi.org/10.1186/s13046-018-0750-2

[21] Z. Liu, L. Qi, Y. Li, X. Zhao, B. Sun, *BMC Cancer* **2017**, *17*, 593. https://doi.org/10.1186/s12885-017-3578-9

[22] M. Zhong, N. Li, X. Qiu, Y. Ye, H. Chen, J. Hua, P. Yin, G. Zhuang, *Int. J. Biol. Sci.* **2020**, *16*, 272. https://doi.org/10.7150/ijbs.37906

[23] R. Aesoy, B. C. Sanchez, J. H. Norum, R. Lewensohn, K. Viktorsson, B. Linderholm, *Mol. Cancer Res.* **2008**, *6*, 1630. https://doi.org/10.1158/1541-7786.MCR-07-2172

[24] S. Svensson, K. Jirström, L. Rydén, G. Roos, S. Emdin, M. C. Ostrowski, G. Landberg, *Oncogene* **2005**, *24*, 4370. https://doi.org/10.1038/sj.onc.1208626

[25] Q.-Q. Xie, H.-Z. Xie, J.-X. Ren, L.-L. Li, S.-Y. Yang, *J. Mol. Graph. Model.* **2009**, *27*, 751. https://doi.org/10.1016/j.jmgm.2008.11.008

[26] R. N. Eskander, K. S. Tewari, *Oncology* **2014**, *132*, 496. https://doi.org/10.1016/j.ygyno.2013.11.029

[27] V. A. Machado, D. Peixoto, R. Costa, H. J. C. Froufe, R. C. Calhelha, R. M. V. Abreu, I. C. F. R. Ferreira, R. Soares, M.-J. R. P. Queiroz, *Bioorg. Med. Chem.* **2015**, *23*, 6497. https://doi.org/10.1016/j.bmc.2015.08.010

[28] J. Dietrich, C. Hulme, L. H. Hurley, *Bioorg. Med. Chem.* **2010**, *18*, 5738. https://doi.org/10.1016/j.bmc.2010.05.063

[29] M. A. Aziz, R. A. T. Serya, D. S. Lasheen, A. K. Abdel-Aziz, A. Esmat, A. M. Mansour, A. N. B. Singab, K. A. M. Abouzid, *Sci. Rep.* **2016**, *6*, 24460. https://doi.org/10.1038/srep24460

[30] L. Zhang, Y. Shan, X. Ji, M. Zhu, C. Li, Y. Sun, R. Si, X. Pan, J. Wang, W. Ma, B. Dai, B. Wang, J. Zhang, *Oncotarget* **2017**, *8*, 104745. https://doi.org/10.18632/oncotarget.20065

[31] V.-J. Claudio, E. J. Barreiro, C. A. M. Fraga, *Curr. Med. Chem.* **2007**, *14*, 1829. https://doi.org/10.2174/092986707781058805

[32] S. Sana, V. G. Reddy, S. Bhandari, T. S. Reddy, R. Tokala, A. P. Sakla, S. K. Bhargava, N. Shankaraiah, *Eur. J. Med. Chem.* **2020**, *200*, 112457. https://doi.org/10.1016/j.ejmech.2020.112457

[33] V. G. Reddy, T. S. Reddy, C. Jadala, M. S. Reddy, F. Sultana, R. Akunuri, S. K. Bhargava, D. Wlodkowic, P. Srihari, A. Kamal, *Eur. J. Med. Chem.* **2019**, *182*, 111609. https://doi.org/10.1016/j.ejmech.2019.111609

[34] K. El-Adl, A.-G. A. El-Helby, H. Sakr, A. Elwan, *New J. Chem.* **2020**, *45*, 881. https://doi.org/10.1039/d0nj02990d

[35] K. El-Adl, M.-K. Ibrahim, M. S. I. Alesawy, I. H. Eissa, *Bioorg. Med. Chem.* **2021**, *30*, 115958. https://doi.org/10.1016/j.bmc.2020.115958

[36] M. A. El-Zahabi, H. Sakr, K. El-Adl, M. Zayed, A. S. Abdelraheem, S. I. Eissa, H. Elkady, I. H. Eissa, *Bioorg. Chem.* **2020**, *104*, 104218. https://doi.org/10.1016/j.bioorg.2020.104218

[37] A. Turky, A. H. Bayoumi, A. Ghiaty, A. S. El-Azab, A. A.-M. Abdel-Aziz, H. S. Abulkhair, *Bioorg. Chem.* **2020**, *101*, 104019. https://doi.org/10.1016/j.bioorg.2020.104019

[38] H. S. Abulkhair, A. Turky, A. Ghiaty, H. E. A. Ahmed, A. H. Bayoumi, *Bioorg. Chem.* **2020**, *100*, 103899. https://doi.org/10.1016/j.bioorg.2020.103899

[39] K. El-Adl, A.-G. A. El-Helby, H. Sakr, A. Elwan, *Bioorg. Chem.* **2020**, *105*, 104399.

[40] I. H. Eissa, A. A. El-Helby, H. A. Mahdy, M. M. Khalifaa, H. A. Elnagar, A. B. M. Mehany, A. M. Metwaly, M. A. Elhendawy, M. M. Radwan, M. A. ElSohly, K. El-Adl, *Bioorg. Chem.* **2020**, *105*, 104380. https://doi.org/10.1016/j.bioorg.2020.104380

[41] N. M. Saleh, M. S. A. El-Gaby, K. El-Adl, N. E. A. Abd El-Sattar, *Bioorg. Chem.* **2020**, *104*, 104350. https://doi.org/10.1016/j.bioorg.2020.104350

[42] K. El-Adl, A. A. El-Helby, H. Sakr, S. El-Hddad, *Arch. Pharm. (Weinheim)* **2020**, *353*, e2000068. https://doi.org/10.1002/ardp.202000068

[43] K. El-Adl, A. A. El-Helby, R. R. Ayyad, H. A. Mahdy, M. M. Khalifa, H. A. Elnagar, A. B. M. Mehany, A. M. Metwaly, M. A. Elhendawy, M. M. Radwan, M. A. ElSohly, I. H. Eissa, *Bioorg. Med. Chem.* **2020**, *29*, 115872. https://doi.org/10.1016/j.bmc.2020.115872

[44] A. A. El-Helby, H. Sakr, I. H. Eissa, A. A. Al-Karmalawy, K. El-Adl, *Arch. Pharm. (Weinheim)* **2019**, *352*, 1900178. https://doi.org/10.1002/ardp.201900178

[45] A.-G. A. El-Helby, R. R. A. Ayyad, H. Sakr, K. El-Adl, M. M. Ali, F. Khedr, *Arch. Pharm. (Weinheim)* **2017**, *350*, 1700240. https://doi.org/10.1002/ardp.201700240

[46] A.-G. A. El-Helby, R. R. A. Ayyad, H. Sakr, K. El-Adl, M. M. Ali, F. Khedr, *Anticancer Agents Med. Chem.* **2018**, *18*, 1184. https://doi.org/10.2174/1871520618666180412123833

[47] A. A. El-Helby, H. Sakr, I. H. Eissa, H. Abulkhair, A. A. Al-Karmalawy, K. El-Adl, *Arch. Pharm. (Weinheim)* **2019**, *352*, 1900113. https://doi.org/10.1002/ardp.201900113

[48] M. McTigue, B. W. Murray, J. H. Chen, Y.-L. Deng, J. Solowiej, R. S. Kania, *Proc. Natl. Acad. Sci. U. S. A.* **2012**, *109*, 18281. https://doi.org/10.1073/pnas.1207759109

[49] A. A. El-Helby, R. R. A. Ayyad, M. F. Zayed, H. S. Abulkhair, H. Elkady, K. El-Adl, *Arch. Pharm. (Weinheim)* **2019**, *352*, 1800387. https://doi.org/10.1002/ardp.201800387
[50] A. Turky, A. H. Bayoumi, F. F. Sherbiny, K. El-Adl, H. S. Abulkhair, *Mol. Divers.* **2021**, *25*, 403. https://doi.org/10.1007/s11030-020-10131-0
[51] H. Abul-Khair, S. Elmeligie, A. Bayoumi, A. Ghiaty, A. El-Morsy, M. H. Hassan, *J. Heterocycl. Chem.* **2013**, *50*, 1202. https://doi.org/10.1002/jhet.714
[52] A. G. A. El-Helby, R. R. Ayyad, H. M. Sakr, A. S. Abdelrahim, K. El-Adl, F. S. Sherbiny, I. H. Eissa, M. M. Khalifa, *J. Mol. Struct.* **2017**, *1130*, 333. https://doi.org/10.1016/j.molstruc.2016.10.052
[53] M. H. El-Shershaby, K. M. El-Gamal, A. H. Bayoumi, K. El-Adl, H. E. A. Ahmed, H. S. Abulkhair, *Arch. Pharm. (Weinheim)* **2021**, *354*, e2000277. https://doi.org/10.1002/ardp.202000277
[54] A. M. El-Morsy, M. S. El-Sayed, H. S. Abulkhair, *Open J. Med. Chem.* **2017**, *07*, 1. https://doi.org/10.4236/ojmc.2017.71001
[55] A. Turky, F. F. Sherbiny, A. Bayoumi, H. E. A. Ahmed, H. S. Abulkhair, *Arch. Pharm. (Weinheim)* **2020**, *353*, e2000170. https://doi.org/10.1002/ardp.202000170
[56] S. Ihmaid, H. E. A. Ahmed, A. Al-Sheikh Ali, Y. E. Sherif, H. M. Tarazi, S. M. Riyadh, M. F. Zayed, H. S. Abulkhair, H. S. Rateb, *Bioorg. Chem.* **2017**, *72*, 234. https://doi.org/10.1016/j.bioorg.2017.04.014
[57] A. M. Omar, S. Ihmaid, E.-S. E. Habib, S. S. Althagfan, S. Ahmed, H. S. Abulkhair, H. E. A. Ahmed, *Bioorg. Chem.* **2020**, *99*, 103781. https://doi.org/10.1016/j.bioorg.2020.103781
[58] K. M. El-Gamal, M. S. Hagrs, H. S. Abulkhair, *Bull. Fac. Pharm. (Cairo Univ.)* **2016**, *54*, 263. https://doi.org/10.1016/j.bfopcu.2016.08.002
[59] T. Mosmann, *J. Immunol. Methods* **1983**, *65*, 55.
[60] D. E. V. Pires, T. L. Blundell, D. B. Ascher, *J. Med. Chem.* **2015**, *58*, 4066. https://doi.org/10.1021/acs.jmedchem.5b00104
[61] C. A. Lipinski, F. Lombardo, B. W. Dominy, P. J. Feeney, *Adv. Drug Deliv. Rev.* **1997**, *23*, 3. https://doi.org/10.1016/S0169-409X(96)00423-1
[62] A. Beig, R. Agbaria, A. Dahan, *PLOS One* **2013**, *8*, e68237. https://doi.org/10.1371/journal.pone.0068237
[63] A. AbdelHaleem, A. O. Mansour, M. AbdelKader, R. K. Arafa, *Bioorg. Chem.* **2020**, *103*, 104222. https://doi.org/10.1016/j.bioorg.2020.104222
[64] B. Baum, M. Mohamed, M. Zayed, C. Gerlach, A. Heine, D. Hangauer, G. Klebe, *J. Mol. Biol.* **2009**, *390*, 56. https://doi.org/10.1016/j.jmb.2009.04.051
[65] A.-G. A. El-Helby, R. R. A. Ayyad, K. El-Adl, H. Sakr, A. A. Abd-Elrahman, I. H. Eissa, A. Elwan, *Med. Chem. Res.* **2016**, *25*, 3030. https://doi.org/10.1007/s00044-016-1723-7
[66] A.-G. A. El-Helby, R. R. A. Ayyad, K. El-Adl, H. Elkady, *Mol. Divers.* **2019**, *23*, 283. https://doi.org/10.1007/s11030-018-9871-y
[67] M. Ferrari, M. C. Fornasiero, A. M. Isetta, *J. Immunol. Methods* **1990**, *131*(2), 165. https://doi.org/10.1016/0022-1759(90)90187-z
[68] D. R. Appling, *J. Am. Chem. Soc.* **2008**, *130*, 6056. https://doi.org/10.1021/ja801998j
[69] L. Zhong, X.-N. Guo, X.-H. Zhang, Q.-M. Sung, L.-J. Tong, Z.-X. Wu, X.-M. Luo, H.-L. Jiang, F.-J. Nan, X. Zhang, L.-P. Lin, J. Ding, *Cancer Biol. Ther.* **2006**, *5*, 323. https://doi.org/10.4161/cbt.5.3.2543
[70] PerkinElmer Inc, VEGF (human) AlphaLISA Detection Kit, 500 Assay Points (2020). https://www.perkinelmer.com/product/alphalisa-vegf-research-kit-500-tests-al201c (accessed: September **2020**).

SUPPORTING INFORMATION

Additional Supporting Information may be found online in the supporting information tab for this article.

How to cite this article: K. El-Adl, H. Sakr, S. S. A. El-Hddad, A.-G. A. El-Helby, M. Nasser, H. S. Abulkhair, *Arch. Pharm.* **2021**, e2000491.